On the Participation of Photo-induced N-H Bond Fission in Aqueous Adenine at 266 and 220 nm: A Combined Ultrafast Transient Electronic and Vibrational Absorption Spectroscopy Study

Gareth M. Roberts,* Hugo Marroux, Michael P. Grubb, Michael N. R. Ashfold and Andrew J. Orr-Ewing*

School of Chemistry, University of Bristol, Cantock's Close, Bristol, BS8 1TS, UK

*Correspondence emails: g.m.roberts@bristol.ac.uk; a.orr-ewing@bristol.ac.uk

Abstract

A combination of ultrafast transient electronic absorption spectroscopy (TEAS) and transient vibrational absorption spectroscopy (TVAS) is used to investigate whether photo-induced N–H bond fission, mediated by a dissociative $^1\pi\sigma^*$ state, is active in aqueous adenine (Ade) at 266 and 220 nm. In order to isolate UV/visible and IR spectral signatures of the adeninyl radical (Ade[-H]), formed as a result of N-H bond fission, TEAS and TVAS are performed on Ade in D_2O under basic conditions (pD = 12.5), which forms Ade[-H]$^-$ anions *via* deprotonation at the N7 or N9 sites of Ade's 7H and 9H tautomers. At 220 nm we observe one-photon detachment of an electron from Ade[-H]$^-$ and identify a threshold of 4.9 ± 0.1 eV (~250 nm) for this process in D_2O, which generates solvated electrons (e^-_{aq}) together with Ade[-H] radicals, with clear signatures in both TEAS and TVAS. Analogous TEAS experiments on aqueous Ade at pD = 7.4 generate a similar photoproduct signal together with e^-_{aq} after excitation at 266 and 220 nm. These e^-_{aq} are born from two-photon ionization of

Ade, together with Ade^+ cations, which are found to be indistinguishable from Ade[-H] radicals in TEAS. Ade^+ and Ade[-H] are found to have different signatures in TVAS and we verify that the pD = 7.4 photoproduct signal observed in TEAS following 220 nm excitation is solely due to Ade^+ cations. Based on these observations, we conclude that: (i) N–H bond fission in aqueous Ade is inactive at ≥220 nm; and (ii) if such a channel exists in aqueous solution, its threshold is strongly blue-shifted relative to the onset of the same process in gas phase 9H-Ade (≤233 nm). In addition, we extract excited state lifetimes and vibrational cooling dynamics for 9H-Ade and $Ade[-H]^-$, which occur within timeframes of <500 fs and 4-5 ps, respectively. In contrast, 7H-Ade is confirmed to have a longer excited state lifetime of ~5-10 ps through both TEAS and TVAS.

1. Introduction

The selection of specific chemical building-blocks for life through evolutionary pressure has received considerable interest within the broader scientific community, particularly with regard to the DNA and RNA nucleobases, which are responsible for encoding our genetics. One central factor, which has been postulated to contribute to this selection process on the early pre-biotic Earth,[1-3] is the resistance that the nucleobases exhibit toward photo-chemical damage following the absorption of solar UV radiation.[4-6] As such, the DNA and RNA nucleobases are classed as photostable species. From a photochemistry perspective, photostability is often characterized by short (<1 ps) electronically excited state lifetimes, low fluorescence quantum yields ($\Phi_f < 10^{-4}$) and a strong resistance to the formation of undesired and potentially harmful photoproducts.[7] Over the past decade, great strides have been made toward understanding the mechanistic origins of nucleobase photostability, using both cutting-edge experimental and theoretical methodologies.[4-6, 8, 9] Together, these studies have revealed that after UV photoexcitation to optically bright electronically excited $^1\pi\pi^*$ states, structural rearrangement allows (often barrierless) access to an array of conical intersections – points of electronic state degeneracy in multi-dimensional nuclear coordinate space[10, 11] – which enable excited state flux to repopulate the singlet electronic ground state (S_0), both rapidly and non-radiatively. This ultrafast (sub-1 ps) relaxation process transforms potentially harmful electronic energy into less harmful excess vibrational energy (heat) in S_0, which may then subsequently be quenched to the surrounding solvent bath (typically H_2O in biological systems) through vibrational energy transfer (VET).

Here we focus of the photophysics of the purine derived nucleobase adenine (Ade), shown in Scheme 1. The biologically relevant 9H tautomer of Ade (Scheme 1, blue) has received considerable theoretical attention.[9, 12-30] A number of conical intersections can potentially facilitate repopulation of S_0 from the initially excited $^1\pi\pi^*$ state(s), depending on

the initial excitation energy. There has been some debate regarding the dominant pathway for re-accessing S_0 after UV excitation in 9H-Ade, although the general consensus is that out-of-plane ring distortion at either the C2 or C6 sites (see Scheme 1) leads to conical intersections which facilitate ultrafast (and near barrierless) internal conversion (IC) back to S_0; we note for completeness that recent work suggests direct $^1\pi\pi^* \rightarrow S_0$ IC is likely to be the dominant process,[9, 21, 26, 31] rather than a sequential $^1\pi\pi^* \rightarrow {}^1n\pi^* \rightarrow S_0$ process.[12, 26] In addition to these out-of-plane 'ring-puckering' conical intersections, Domcke and co-workers[14, 32] first proposed that at shorter excitation wavelengths, competing relaxation mechanisms, mediated by conical intersections lying along alternative co-ordinates, may also become active; namely, ring-opening along the C8–N9 bond[14] and homolytic bond fission along the N9–H coordinate (or $N10H_2$ amino group).[14, 17, 18, 21] Both of these channels are driven by the presence of dissociative $^1\pi\sigma^*$ states, which are ubiquitous in aromatic molecules containing heteroatoms (O, N, S *etc*.) and have become an intense area of study within the chemical dynamics community.[32-34] With reference to the schematic potentials in Figure 1, Domcke and co-workers predicted that upon excitation to the $^1\pi\pi^*$ state(s) at energies >5.5 eV (<225 nm), population could couple through a $^1\pi\pi^*/^1\pi\sigma^*$ conical intersection at elongated N9–H distances to access a dissociative $^1\pi\sigma^*$ state.[14] Once on that $^1\pi\sigma^*$ state, population may then traverse a lower energy $^1\pi\sigma^*/S_0$ conical intersection at further extended N9–H bond lengths and either (i) directly form adeninyl radical photoproducts, Ade[-H], in coincidence with translationally excited H-atoms, or (ii) form vibrationally hot Ade in its S_0 state. It is the participation of this N–H bond fission pathway which forms the main thrust of the studies presented in this paper.

Experimental studies of isolated Ade's excited state dynamics in the gas phase have been well documented (see Ref. 35 and references therein). Such an approach has been particularly attractive given that only the canonical 9H-Ade tautomer is present under cold

molecular beam conditions.[35] In general, excited state population of 9H-Ade decays bi-exponentially, with time-constants of ≤100 fs and ~1 ps.[36-39] With specific regard to the participation of the $^1\pi\sigma^*$ state in 9H-Ade's photochemistry, a number of studies have been performed to investigate the activity of this channel.[38-44] Early work in both the time and frequency domains led a number of research groups to infer that ultrafast relaxation *via* this state may in fact be active following excitation at 267 nm;[38, 41, 42] a much longer wavelength than initially predicted by Domcke and co-workers[14] and later theoretical work.[18, 21] However, high-resolution photofragment translational spectroscopy measurements by Nix *et al*. more definitively identified the onset for N9–H bond fission *via* the $^1\pi\sigma^*$ state as ≥5.3 eV (≤233 nm),[43] in-line with findings from more recent time-resolved measurements in the gas phase by both Stavros and co-workers[44] and Ullrich and Evans.[39] Stavros and co-workers also confirmed that by 200 nm, N–H bond fission in the $N10H_2$ amino group is activated and N–H bond scission along both coordinates takes ~100 fs,[44] in general agreement with theory.[14, 21]

The excited state dynamics of Ade in aqueous solution have also been extensively reviewed.[4, 5] Following 266 nm irradiation in H_2O, Kohler and co-workers[45] performed ultrafast transient electronic (UV/visible) absorption spectroscopy (TEAS) measurements on Ade, which identified that 9H-Ade possesses an excited state lifetime of 180 fs. In addition, they confirmed that ~20% of aqueous Ade is present in the 7H tautomer (Scheme 1, red), in accord with NMR measurements.[46, 47] 7H-Ade was found to possess a much longer excited state lifetime of ~8.8 ps,[45] as inferred through selective methylation of Ade, and in-line with observations from later ultrafast measurements.[48] However, unlike gas phase Ade, little is known about competing deactivation *via* the $^1\pi\sigma^*$ state in aqueous Ade, particularly from an experimental perspective. Temps and co-workers performed ultrafast fluorescence up-conversion measurements, exciting between 280 and 245 nm, and found that at ~265 nm 9H-Ade's fluorescence lifetime sharply decreases from ~670 fs to ~340 fs.[49] This led them to

suggest tentatively the onset for accessing the $^1\pi\sigma^*$ surface, but they acknowledged that a host of other phenomena might also give rise to this observation. More recent theory on aqueous 9H-Ade suggests that coupling onto the $^1\pi\sigma^*$ state may start at energies corresponding to much shorter excitation wavelengths than 265 nm, and perhaps even shorter than the experimentally determined 233 nm threshold in isolated 9H-Ade.[18, 31] Furthermore, it may be possible that heterolytic N-H bond cleavage channels open in aqueous Ade, mediated through electron-driven H-atom elimination (EDHE)[50] following (auto-)ionization. EDHE pathways can be enhanced through a suppression of the adiabatic ionization potential (IP) in H_2O,[34] which recent experiments and calculations suggest is reduced by ~1 eV relative to the gas phase.[51-53] Related EDHE behavior has been observed for aqueous 2-aminopurine (a structural isomer of Ade), albeit initiated through two-photon absorption at 266 nm.[54]

Herein, we present new TEAS and transient vibrational absorption spectroscopy (TVAS) studies, which aim to reveal whether N-H bond fission (mediated by the $^1\pi\sigma^*$ state) is active in aqueous Ade after photoexcitation at 266 nm and 220 nm. We show that, only through combined TEAS and TVAS on Ade in D_2O, under *both* neutral (pD = 7.4) and basic (pD = 12.5) conditions (see Scheme 1), can a definitive assignment of any Ade[-H] radicals formed through N–H bond fission be made.

2. Methods

A. Experimental

All transient absorption experiments were performed using a newly commissioned ultrafast laser system at the University of Bristol, a schematic diagram of which is provided in the supporting information (SI) online (Figure S1). The system consists of a Coherent Vitara-S oscillator and Coherent Legend Elite HE+ regenerative amplifier, operating at 1 kHz and configured to produce 40 fs duration pulses at 800 nm with a total output power of 5 W. This

fundamental beam is split into three parts using a series of beam splitters: two parts have energies of 2.45 mJ/pulse, with one much lower energy beam of 100 μJ/pulse. The two 2.45 mJ/pulse beams seed two Coherent OPerA Solo optical parametric amplifiers (OPAs). One of these OPAs produces spectrally tunable light spanning the UV to infrared (IR) range (220 – 20,000 nm) and is used to generate the 266 and 220 nm pump pulses for all our transient absorption experiments. The remaining OPA generates broadband (~300 cm^{-1}) tunable IR pulses for use as our probe in TVAS experiments, with energies of ~1 μJ/pulse at the sample. Finally, the remaining 100 μJ/pulse 800-nm seed is used to generate a broadband white-light continuum (WLC), for use as the probe in TEAS experiment. This WLC probe was generated by focusing the 800-nm seed into a 2-mm thick CaF_2 window with an f = 200 mm focal length CaF_2 lens. The power of the 800 nm seed was further attenuated using a polarizer and series of neutral density filters, while its spatial profile and beam waist were controlled using a series of irises. Continuous rastering of the CaF_2 window in a plane perpendicular to the incident direction of the focused 800 nm seed beam avoided thermal damage. An off-axis parabolic mirror (f = 100 mm) re-collimated the resulting WLC probe, which spans wavelengths from ~320 nm to >800 nm.

For both TEAS and TVAS measurements, the UV pump pulse (either 266 or 220 nm) was attenuated to between ~160 – 200 nJ/pulse by cross-polarization using a λ/2 waveplate and wire-grid polarizer, and then focused ~2 cm behind the sample by a f = 200 mm CaF_2 lens. A beam profiler (Thorlabs, BP209-VIS/M) was used to determine a ~250 μm beam diameter for the Gaussian profile (full-width at half maximum) of the pump beam at the sample, returning pump fluences (F) in the range of $F \approx 0.3 – 0.4$ mJ cm^{-2}. Performing experiments at these low pump fluences ensured there was no undesired production of solvated electrons through non-resonant two-photon ionization of the D_2O solvent[55] (see Section 3A for more details).

For TEAS, the WLC probe pulse was reflectively focused into the sample using a f = 75 mm concave aluminium mirror (to avoid achromatic aberrations) to a tight ~50 μm beam diameter, so that the probed region of the sample was uniformly excited by the more loosely focused UV pump beam. The polarization of the WLC probe was maintained at the magic angle (54.7°), relative to the polarization of the UV pump pulse, by using a λ/2 waveplate in the 800 nm WLC seed beam line. The temporal delay (*t*) between the UV pump and WLC probe pulses was controlled by changing the path length of the pump beam with an aluminum retro-reflector (PLX) mounted on a motorized 220 mm delay stage (Thorlabs, DDS220/M), providing a maximum possible delay of t = 1.3 ns. The pump and probe beams then intersected the sample with a small crossing angle of ~5°. After transmission through the sample, the WLC probe light was collected by an optical fiber, coupled to a CCD spectrometer (Avantes, AvaSpec-DUAL). The spectrometer was able to disperse 200 – 620 nm light over 750 pixels, providing a spectral resolution of 0.5 nm. Prior to interaction with the sample, the UV pump beam was modulated at 500 Hz (blocking every other pulse) with an optical chopper wheel (Thorlabs, MC2000) to obtain pump on/off spectra pairs at each *t*, which are required to generate the individual transient absorption spectra. Data acquisition and calculation of the transient absorption spectra at each *t* was carried out using a custom built LabVIEW program. This program also controlled the motorized delay stage and was set up to sample many values of *t* in a random order, to ensure that long time experimental drifts in signal intensity did not induce artificial kinetics in the data. Chirp-correction of the recorded TEAS datasets was performed using the spectral analysis software package KOALA (see Ref. 56 for further details). Non-resonant two-color two-photon absorption measurements in D_2O,[55] reveal an instrument response function (IRF) of ~110-120 fs in our TEAS measurements (see SI online, Figure S2). This response was predominantly limited by the temporal width of our UV pump pulses, which we do not further temporally compress

after they are generated by the OPA. For TEAS experiments performed at 220 nm this D_2O solvent response was found to contribute significantly to the recorded spectra within the first ~200 fs and solvent only spectra were subtracted from the raw TEAS datasets to remove this solvent-only contribution (see Figure S2d).

TVAS experiments were performed using the same general methodology outlined above for TEAS, but instead implement broadband IR probe pulses, which were generated by difference frequency generation of the signal and idler beams from the IR OPA. The resulting IR probe radiation from this process could be tuned from 1250 – 4000 cm^{-1} with a 300 cm^{-1} bandwidth. For the experiments described here, the IR probe was set to be centered at ~1580 cm^{-1}. The entire IR probe beam line was enclosed by sealed plastic tubes and continuously purged by dry, clean air to avoid undesired absorption by atmospheric H_2O and CO_2. After passing through the sample, the transmitted IR probe light was detected by a 128 pixel, liquid nitrogen cooled Mercury Cadmium Telluride array (Infrared Associates Inc., MCT-10-128) coupled to a spectrometer (HORIBA Scientific, iHR320), providing a spectral resolution of ~5 nm. Prior to interacting with the sample, the IR probe pulse is split into two beams of equal energy, one of which probed the UV pumped sample. The second beam did not pass through the sample and was sent into an identical array detector and spectrometer, so that artificial difference signal resulting from shot-to-shot variations in the spectral profile of the IR probe could be corrected.

6 mM sample solutions of Ade (Sigma-Aldrich, ≥99%) in D_2O (Sigma-Aldrich, 99.9%) were prepared under either neutral (pD = 7.4) or basic conditions (pD = 12 .5), the latter of which was produced by the addition of NaOD (Sigma-Aldrich, 99%) and the determined pH corrected according to the relationship pD = pH + 0.4.[57] These sample solutions were then delivered through a stainless steel flow cell, containing two 1.5 mm thick CaF_2 windows separated by either a 100 or 200 μm thick Teflon spacer, which defines the

absorption path length. The sample solution was flowed continuously through the cell by a peristaltic pump (Cole Parmer, Masterflex) with PTFE tubing throughout, at a flow speed sufficient to ensure fresh solution was sampled with each laser shot (>1 kHz). Comparative experiments were also performed on sample solutions delivered by a windowless wire-guided liquid gravity jet, based on the design by Tauber *et al*.[58] These TEAS experiments were performed to investigate whether there were any undesired effects induced by the CaF_2 windows in the flow cell. Under the conditions described above, identical ultrafast (sub-500 fs) kinetics and spectral profiles were identified for both sample delivering methods. As such, all results presented herein are obtained using the flow cell, which offers greatly improved sample stability over the full duration of experiments relative to the gravity jet.

B. Theory

Density functional theory, with the B3LYP functional,[59, 60] was used to determine the anharmonically corrected vibrational frequencies of all species considered in this study: 9H-Ade, 7H-Ade, 9H-Ade$^+$, 7H-Ade$^+$, the Ade[-H] radical and the deprotonated Ade[-H]$^-$ anion. All anharmonic frequency calculations were determined for species in the gas phase. Ground state geometry optimizations on each of these species was performed at the B3LYP/6-311+G(d,p) level of theory and verified as minima through further anharmonically corrected frequency calculations (no imaginary frequencies). Time-dependent density functional theory was also used to calculate the electronic absorption profiles of aqueous 9H-Ade$^+$, 7H-Ade$^+$, neutral Ade[-H] radical and Ade[-H]$^-$ anion. Following ground state geometry optimization at the PBE0/aug-cc-pVTZ level of theory, vertical excitation energies of the first 20 electronic transitions for these species were determined using TD-PBE0/aug-cc-pVTZ calculations. Electrostatic effects of aqueous solvation was taken into account using a polarizable continuum model, while the PBE0 functional[61] was selected for its balanced description of both excited valence and charge-transfer/Rydberg states, as shown by Leang *et al*,[62] and its

reasonable description of electronic transitions in Ade.[29] All calculations were performed using the Gaussian09 computational package.[63]

3. Results & Analysis

A. Transient Electronic Absorption of Deprotonated Adenine at 266 nm

We begin by considering measurements on a 6 mM solution of Ade in D_2O under basic conditions (pD = 12.5). As shown in Scheme 1, the proton attached to the N9 and N7 sites of 9H-Ade and 7H-Ade possesses a known pK_a of 9.8[64, 65] and solvation of Ade in D_2O under these basic conditions will lead to formation of deprotonated adenine anions, Ade[-H]$^-$ (Scheme 1). In aqueous Ade[-H]$^-$ any possibility of photo-induced bond fission along the N(9/7)–H coordinates is necessarily removed and experiments on this deprotonated species will serve as an important benchmark for comparison with photoexcited Ade in D_2O at pD = 7.4, where N–H bond fission may become an active channel.

The results of TEAS measurements following photoexcitation of aqueous Ade[-H]$^-$ with a 266 nm (4.66 eV) fs pump pulse and probing with a broadband white-light continuum (340 – 620 nm) are presented in Figures 2a – c. The chirp-corrected TEA spectra obtained from these experiments are presented as a false-color intensity plot in Figure 2a, between time-delays (*t*) of –200 fs and 3 ps. Around t = 0 ps, a broad transient absorption signal spanning the full range of our probe window is observed, which peaks at ~420 nm. In order to assign this signal, we first make reference to the static UV absorption spectrum of aqueous Ade[-H]$^-$, which is shown inset in Figure 1 (green line). The static spectrum shows that, while the absorption profile of Ade[-H]$^-$ is red-shifted relative to neutral Ade (blue line), it does not extend into our TEAS probe window. This leads us to conclude that the spectral shape of the transient absorption in Figure 2a is not influenced by any overlapping bleach signal from Ade[-H]$^-$. Instead, based on comparison with previous literature for Ade and its

derivatives[45, 66, 67] we assign this signal purely to excited state absorption (ESA) from initially excited bright $^1\pi\pi^*$ state(s) to higher lying singlet states (see SI, Figure S3). After t = 0 ps, no obvious evolution in the spectral shape of this ESA signal is observed, but rather it simply decays back to the zero baseline by t = 3 ps, in a monotonic manner. A kinetic trace through a 5 nm wide slice of this ESA signal at λ_{probe} = 400 nm is shown in Figure 2b, which returns a single time-constant of 470 ± 18 fs when fitted with an exponential decay convoluted with our 120 fs Gaussian IRF. This time-constant reports the excited state lifetime of Ade[-H]$^-$, and demonstrates that, like neutral 9H-Ade in D_2O (*vide infra*),[45] population initially imparted to the $^1\pi\pi^*$ state(s) still decays on an ultrafast timescale.

Finally, Figure 2c presents select TEA spectra at longer time-delays ($t \geq$ 950 fs), which illustrate that after the ESA signal has decayed by $t \approx$ 3 ps, no further absorption signal persists within our probe window, out to the longest recorded time-delay of t = 100 ps. This may suggest that there is no significant photoproduct yield after irradiation of aqueous Ade[-H]$^-$ at 266 nm. In particular, there is no signature of photodetachment/ionization from either Ade[-H]$^-$ or D_2O, which at the very least would generate solvated electrons, e^-_{aq}, with a well-known broad absorption increasing towards the red end of our probe window (λ_{max} ~ 715 nm in water[68]). The absence of any e^-_{aq} accords with the fact that our experiments are conducted with sufficiently low pump fluences ($F \approx$ 0.3 mJ cm^{-2}) that the formation of e^-_{aq} through non-resonant two-photon ionization of D_2O is negligible (*cf.* Ref. 55). The representative D_2O solvent only trace at t = 500 ps in Figure 2c (dashed grey line) also exhibits no e^-_{aq} signal.

B. Transient Vibrational Absorption of Deprotonated Adenine at 266 nm

In addition to TEAS measurements, TVAS has been performed to gain insight into the subsequent vibrational cooling dynamics of Ade[-H]$^-$ in its S_0 electronic ground state, following IC from the $^1\pi\pi^*$ state(s). Figure 2d presents TVA spectra of Ade[-H]$^-$ (6 mM)

from t = 0 – 20 ps, across a probe window of 1490 – 1680 cm^{-1}. Within this window, two bleach features are observed at the earliest time-delays, centered at 1538 cm^{-1} and 1612 cm^{-1}, which reflect population transfer out of S_0 to the $^1\pi\pi^*$ state(s) by the 266 nm pump. Assignment of these features to specific vibrational modes is guided by frequency calculations on gas phase Ade[-H]$^-$ at the B3LYP/6-311+G(d,p) level, in addition to comparison with previous vibrational assignments in Ade (*vide infra*).[69-71] Our calculations determine a number of vibrations in this region, the strongest of which belongs to a mode dominated by an in-plane scissoring motion of the NH_2 group (ν_{scis}), predicted at 1596 cm^{-1}. We therefore assign the stronger of these two bleaches at 1612 cm^{-1} to ν_{scis}, while the most likely assignment of the weaker bleach at 1538 cm^{-1} is to an in-plane ring-stretching motion (ν_{rs}), predicted at 1507 cm^{-1}. As we show later, both of these modes have analogues in 7H- and 9H-Ade, for which our B3LYP frequency calculations prove to be more faithful.

Positive transient absorptions are also observed to lower wavenumber of both the ν_{scis} and ν_{rs} features in Figure 2d, which then shift to higher wavenumber and decay within the first 10 ps. Based on this distinctive behavior, we assign them to highly vibrationally excited ν_{scis} and ν_{rs} in S_0 (hereon termed ν^*_{scis} and ν^*_{rs}), formed immediately after ultrafast IC (~500 fs) from the excited $^1\pi\pi^*$ state(s). The kinetics for the blue-shifts of ν^*_{scis} and ν^*_{rs} are extracted by fitting these features to Gaussian functions (of fixed widths) in each individual TVA spectrum, using the kinetics analysis software package KOALA.[56] The peak center shifts extracted from this process are presented in Figure 2e, up to t = 8 ps, which show that ν^*_{scis} blue-shifts by ~30 cm^{-1} from 1575 cm^{-1}, while ν^*_{rs} shifts from ~1520 to ~1535 cm^{-1}. Both shifts are well described by fits to single exponentials, with time-constants of 1.7 ± 0.4 ps and 1.1 ± 0.3 ps for ν^*_{scis} and ν^*_{rs}, respectively. In-line with very recent TVAS studies by Murdock *et al.*,[72] we assign these time-constants to the *average* timescale for vibrational

cooling from highly vibrationally excited levels (v >> 1) in the S_0 state of Ade[-H]$^-$, *via* rapid VET to solvent bath modes. The picture put forward for vibrational cooling by Murdock *et al*. also takes the final v = 1 → v = 0 step to be rate limiting and gives rise to a distinctive sigmoidal-like profile for the recovery of the associated bleaches. This behavior is seen in Figure 2f, which presents kinetic traces for the recovery of both bleaches, obtained by simple integration of the bleach signals. In both cases, recovery is clearly delayed by ~1-2 ps, due to the time required for population in v >> 1 levels to cool back down to v = 1, prior to repopulation of the final v = 0 level in S_0. Kinetic fits with an appropriate sigmoid function[72] (see SI for details) provide time-constants of 1.9 ± 0.2 ps and 2.2 ± 0.7 ps for the final v = 1 → v = 0 cooling step in the ν_{scis} and ν_{rs} modes of Ade[-H]$^-$, respectively. A very small fraction (~3%) of these bleaches does not recover by t = 30 ps, which is most clearly seen from Figure 2f. Although no new absorption features are observed in either our TVAS or TEAS at 266 nm, the incomplete bleach recovery could hint at a very small quantum yield for photoproduct formation, but we acknowledge that such a minimal offset in bleach recovery may also be due to thermal effects in the D_2O solvent bath induced by the pump pulse.[7, 73] We explore the possibility of photoproduct formation further in the next section.

C. Transient Absorption of Deprotonated Adenine at 220 nm

TEAS and TVAS have also been performed on aqueous Ade[-H]$^-$ (6 mM, pD = 12.5) following excitation at the much shorter pump wavelength of 220 nm (5.64 eV), which imparts an additional ~1 eV of excess energy to Ade[-H]$^-$, relative to 266 nm. Excitation at 220 nm will initially populate higher lying bright $^1\pi\pi^*$ states(s) of Ade[-H]$^-$ (see SI), which give rise to a new absorption band at <235 nm in its static UV absorption spectrum (Figure 1, inset). The results of these studies are collated in Figure 3 and we first consider TEAS at 220 nm. The chirp-corrected TEA spectra, after subtraction of a D_2O solvent response, are

presented in Figure 3a and are similar to those observed at 266 nm. We once again assign the transient absorption signal appearing at t = 0 ps to ESA, which then decays with a single time-constant of 420 ± 22 fs (see Figure S4a for kinetic trace at λ_{probe} = 400 nm).

Unlike TEAS at 266 nm, selected TEA spectra in Figure 3b show that after the ESA signal has completely decayed following 220 nm excitation ($t \geq 3.5$ ps), two new, but small, transient absorption signatures are present between 340 – 360 nm and 450 – 620 nm, which persist out to the maximum recorded delay of t = 100 ps. Based on comparison with its known absorption profile, we assign the feature in the red end of the TEA spectrum to e^-_{aq} (*vide supra*). We also re-emphasize that the experiments here are conducted under conditions where e^-_{aq} formation from the D_2O solvent is suppressed, leading us to assert confidently that these e^-_{aq} must be formed through photodetachment from aqueous Ade[-H]$^-$. Additional TEAS experiments, which are provided in the SI online (Figure S5), return an approximate threshold energy of 4.9 ± 0.1 eV (~250 nm) for one-photon electron detachment from Ade[-H]$^-$ in D_2O (*cf*. theoretical values of ~3.2 eV for gas phase Ade[-H]$^-$[74, 75]).

Removal of an electron from Ade[-H]$^-$ will necessarily generate a pair of photoproducts: Ade[-H] + e^-_{aq}. Matrix isolation studies have recently indicated that the neutral Ade[-H] radical, which partners e^-_{aq}, should absorb strongly from 300 – 400 nm and more weakly around ~550 nm.[76] Figure 3c shows that these experimental observations are also consistent with the calculated absorption profile of aqueous Ade[-H] (grey bars) at the TD-PBE0/aug-cc-pVTZ level, as well as other theoretical methods.[77] Together, this evidence leads us to conclude that the persisting absorption signature between 340 and 360 nm in Figure 3b after $t \approx 10$ ps is indeed due to the red-edge of the 300 – 400 nm absorption band of neutral Ade[-H] radicals. An example TEA spectrum at t = 10 ps is overlaid in Figure 3c for comparison. We note that the predicted absorption at ~550 nm for Ade[-H] is most likely

convoluted with e^-_{aq} signal. Moreover, there appears to be some depletion in the Ade[-H] absorption signature at $t \geq 3.5$ ps in Figure 3b, which may be due to some fraction of the Ade[-H] + e^-_{aq} product pair undergoing geminate recombination back to the Ade[-H]$^-$ anion (*cf.* studies in Refs 78 and 79), although a quantitative analysis of these kinetics is not a focus of this work.

The results of TVAS on Ade[-H]$^-$ at 220 nm are presented in Figures 3d and 3e, and return all of the features reported above for 266 nm excitation: a ν_{rs} bleach at 1538 cm^{-1}, a ν_{scis} bleach at 1612 cm^{-1} and positive ν^*_{scis} and ν^*_{rs} hot bands, initially centered at ~1575 and ~1520 cm^{-1}, respectively. The kinetic traces and time-constants for the evolution of each of these features (determined using the same methods outlined in Section 3B) are found to be very similar to those extracted at 266 nm. The time-constants obtained from this analysis are collated in Table 1, together with all other time-constants determined from our measurements in this study, while plots of the kinetic traces are available in the SI (Figure S4). More significantly, both TVA spectra and kinetic traces show that less of the bleach signals recover at 220 nm, returning a larger photoproduct quantum yield of ~8% at this shorter wavelength, in-line with the clear signature of Ade[-H] + e^-_{aq} photoproducts through TEAS. Additionally, two new signals, centered at ~1587 and ~1550 cm^{-1}, are also observed in the TVA spectra for 220 nm excitation, after the hot band dynamics and bleach recovery are complete ($t > 10$ ps). In accordance with our photoproduct assignment in the TEA spectra, we attribute these new features to vibrations of the neutral Ade[-H] radical, formed after photodetachment. To help verify this assignment, we turn to B3LYP frequency calculations on the isolated Ade[-H] radical (Figure 3f), which predict three reasonably strong vibrations within our probe window (shown in Figures 3g-i), the strongest of which belongs to a ν_{scis} mode at 1607 cm^{-1}. These calculations are also in reasonable agreement with the location of modes assigned to Ade[-H] through matrix isolation.[76] This analysis leads us to assign the feature at ~1550 cm^{-1} in our

TVA spectra to a ν_{rs} mode of Ade[-H] (Figures 3i), while the peak at ~1587 cm^{-1} may be due to either: (i) the ν_{scis} mode of Ade[-H] (Figure 3g) which is partially overlapped with the ν_{scis} bleach of $Ade[-H]^-$; or (ii) a second ν_{rs} mode of Ade[-H] (Figure 3i). In the case of the latter, this would suggest that the ν_{scis} product vibration is *directly* (rather than partially) overlapped with the ν_{scis} bleach of $Ade[-H]^-$ at 1612 cm^{-1}. In both scenarios though, overlap between product and bleach features means the photodetachment quantum yield of ~8% extracted from our bleach recovery should be treated as an *absolute lower limit* for this value.

D. Transient Electronic Absorption of Adenine at 266 nm

Armed with UV/Visible and IR spectral signatures for the Ade[-H] radical, we can now begin to investigate whether N-H bond fission in neutral Ade is an active process in aqueous solution down to 220 nm. Once again, we start by considering TEAS, performed on a 6 mM solution of Ade in D_2O, under neutral conditions (pD = 7.4), after excitation at 266 nm. The chirp-corrected TEA spectra obtained from these experiments are presented in Figure 4a, between –200 fs and 200 ps. As with measurements on $Ade[-H]^-$, at t = 0 ps a broad transient absorption signal appears due to ESA from the initially populated $^1\pi\pi^*$ states(s).[45, 66] The ESA feature for Ade exhibits two discernable peaks, the more intense of which is initially centered at ~380 nm and then blue-shifts toward ~360 nm within the first 100 – 200 fs. We speculate that this ultrafast spectral evolution may be due to either: (i) rapid motion of the excited state wavepacket relaxing towards a conical intersection geometry with S_0;[25, 26] or (ii) an ultrafast response/reorganization of the surrounding D_2O solvent, as has been observed in other systems.[80-82] More generally, much of the ESA signal decays rapidly within the first ~500 fs, although complete decay back to a baseline level of $m\Delta OD = 0$ is not observed within this time window. Instead some fraction of the ESA signal persists and decays over a much longer timeframe of picoseconds.

The temporal evolution of Ade's ESA feature is more quantitatively depicted in Figures 4b and 4c. The ESA decay trace at λ_{probe} = 580 nm (Figure 4b) compares favorably to that previously reported by Kohler and co-workers at a similar λ_{probe},[45] and a bi-exponential fit (convolved with our IRF) returns time-constants of 200 ± 50 fs (blue line) and 10.3 ± 5 ps (red line). At 580 nm though, an additional long-time signal offset is also observed, due to the formation of e^-_{aq}, which is taken into account for the fit[45, 83] (dashed grey line); we discuss the origins of e^-_{aq} further below. At λ_{probe} = 400 nm (Figure 4c), no e^-_{aq} signal contaminates the ESA, which decays back to a final value of zero with time-constants of 205 ± 14 fs and 5.4 ± 0.7 ps, in reasonable agreement with the fits at 580 nm. In accordance with previous studies,[45, 48] we assign these two time-constants to the excited state lifetimes of the 9H and 7H tautomers of Ade present in D_2O. We note that recent theory on the less studied 7H-Ade now suggests that its significantly longer lifetime may be born from a deeper potential minimum in the excited $^1\pi\pi^*$ (^1L_b) state, which encourages population to decay *via* a slower (barriered) $^1\pi\pi^* \rightarrow {}^1n\pi^* \rightarrow S_0$ pathway, rather than the ballistic movement to a ring-puckering conical intersection with S_0 seen in 9H-Ade.[16, 84]

Figure 4d shows select TEA spectra recorded at $t \geq 3.5$ ps and more clearly reveals that after complete decay of the ESA from 7H-Ade ($t \geq 35$ ps), new transient absorption signatures are present, which do not decay further (within the signal-to-noise) out to the maximum recorded delay of t = 300 ps. Both of these signals are reminiscent of those seen for Ade[-H] + e^-_{aq} photoproducts formed through one-photon electron detachment from Ade[-H]$^-$ at 220 nm (Figure 3b). It is therefore tempting to simply assign the feature at 340 – 360 nm to Ade[-H] radicals, born from homolytic N–H bond fission *via* the $^1\pi\sigma^*$ state, although the presence of e^-_{aq} informs us that some fraction of Ade must also undergo photoionization (given that D_2O is not ionized here, *vide supra*). Considering the latter pathway, it is noteworthy that recent high-level theory[51] and experiment[52, 53] show that Ade's

IP is only suppressed to 7.5 eV in water (*cf.* 8.48 eV in the gas phase[85, 86]). Unlike the above studies on deprotonated Ade[-H]$^-$ anions (which yields no e^-_{aq} signal at 266 nm), removal of an electron from neutral aqueous Ade must therefore occur *via* absorption of two 266 nm (4.66 eV) photons, which is likely resonance-enhanced by initial absorption to the bright $^1\pi\pi^*$ state(s). The resonant nature of this process helps to explain why two-photon ionization of neutral Ade is still observed here, even under conditions where *non-resonant* two-photon ionization of the D_2O solvent (which is in vast excess) is still suppressed. Moreover, given that the initial $^1\pi\pi^* \leftarrow S_0$ absorption cross-sections for both Ade and Ade[-H]$^-$ at 266 nm are similar (see inset Figure 1), we suggest that the absence of two-photon induced electron detachment from Ade[-H]$^-$ at 266 nm is due to a reduced photodetachment cross-section from its intermediate $^1\pi\pi^*$ state, relative to that of neutral Ade's.

Photoionization of Ade will also generate Ade$^+$ cations and further consideration of this possibility makes assignment of the 340 – 360 nm photoproduct signature more challenging. Figure 5a shows the calculated absorption profiles for both aqueous 9H-Ade$^+$ (blue bars) and 7H-Ade$^+$ (red bars) at the TD-PBE0/aug-cc-pVTZ level, in addition to the Ade[-H] radical (grey bars). These results indicate that both cations should absorb at <350 nm and ~500 nm, and would be indistinguishable from Ade[-H] radicals in our TEAS measurements, based on their spectral signatures alone. Given that photoionization must be active here, it is tempting to suggest that at least some of the 340 – 360 nm signal is due to Ade$^+$ cations. However, the cation may not be the final product of this ionization process: it is possible the cation is merely an intermediate species in an ultrafast EDHE process involving the N(9/7)–H coordinate, which would ultimately yield the neutral Ade[-H] radical (*cf.* 2-aminopurine[54]). This third possibility only serves to complicate further a definitive photoproduct assignment. In principle, any temporal evolution of the product signal at 350 nm, together with those of e^-_{aq}, might have helped to disentangle these processes, although

the strong ESA signal from excited Ade prohibits such analysis. Thus, TEAS alone leaves us with an unresolved picture of the final molecular photoproducts formed at 266 nm.

E. Transient Vibrational Absorption of Adenine at 266 nm

In an attempt to shed further light on the molecular photoproducts formed at 266 nm, TVAS has also been performed. Figure 4e presents these TVA spectra of Ade in D_2O (6 mM) from t = 0 – 20 ps. Two bleach features are observed at t = 0 ps, located at 1515 cm^{-1} and 1622 cm^{-1}, due to population transfer out of S_0. As with TVAS on Ade[-H]$^-$, we designate these features to specific vibrational modes through a comparison with B3LYP frequency calculations on both gas phase 9H-Ade and 7H-Ade, which are presented in Figure 5b (blue and red lines, respectively), as well as comparison with previous literature.[70, 71] These lead us to assign the weaker bleach at 1515 cm^{-1} to a ν_{rs} mode of 7H-Ade (Figure 5e), given that only 7H-Ade is calculated to possess any intense vibrations in the range 1490 – 1600 cm^{-1}. Further weight to this assignment comes from TVAS on adenosine (see SI online, Figure S6) and Ade selectively methylated at the N9 position,[5] neither of which can tautomerize and only display strong bleaches at ~1622 cm^{-1}. The stronger bleach at 1622 cm^{-1} is predominantly due to a ν_{scis} vibration in 9H-Ade (Figure 5c), although our calculations indicate that some contribution must also come from the analogous ν_{scis} mode in 7H-Ade (Figure 5d), which is calculated to be less intense (by a factor of ~0.6) and blue-shifted relative to 9H-Ade ν_{scis} by only ~10 cm^{-1}. A positive transient absorption is also observed on the red-edge of the ν_{scis} bleach in Figure 4e, which can be assigned to ν^*_{scis}. From a simple kinetics perspective, in order to observe any significant population density of vibrationally hot S_0 species in TVAS, the timescale for IC from the excited state, τ_{IC}, must be significantly faster than any subsequent vibrational cooling in S_0, τ_{vc} (*i.e.* $\tau_{IC} << \tau_{vc}$). The latter process occurs on the order of picoseconds in D_2O (*vide supra* and Table 1), while TEAS in Section 3D showed

that ultrafast $^1\pi\pi^* \rightarrow S_0$ IC is only observed for 9H-Ade (~200 fs). This leads us to conclude that the ν^*_{scis} feature in Figure 4e is only associated with 9H-Ade. We also highlight that the 7H-Ade ν_{rs} bleach at 1515 cm^{-1} does not share an associated ν^*_{rs} hot band, in-line with our above picture and the much slower IC timescale for 7H-Ade (5-10 ps).

In order to isolate the bleach recovery kinetics of 9H-Ade from 7H-Ade and model the blue-shift of ν^*_{scis}, we performed a fit to each individual TVA spectrum using KOALA.[56] An example fit at t = 1 ps is shown in Figure 4f. Both the 7H-Ade ν_{rs} and ν_{scis} bleaches are modeled using Gaussian functions (red), the relative amplitudes of which are held fixed at a ratio of 1:3 for ν_{rs}:ν_{scis}, based on the calculated IR intensities from B3LYP calculations in Figure 5b. The remaining 9H-Ade ν_{scis} bleach (blue) and ν^*_{scis} hot band (light blue) are also modeled using Gaussians, the latter of which is allowed to float in both amplitude *and* position during fitting. The widths of all Gaussian functions are held fixed throughout.

The first 10 ps of evolution of the ν^*_{scis} peak center shift is shown in Figure 4g. This hot band undergoes a ~25 cm^{-1} blue-shift from its initial location at 1595 cm^{-1} and its kinetics are well described by a single exponential with a time-constant of 2.1 ± 0.2 ps. As discussed previously, we associate this time-constant with the *average* timescale for vibrational cooling in 9H-Ade's S_0 state, driven by VET to the D_2O solvent. The extracted recovery of 9H-Ade's ν_{scis} bleach is also delayed by ~2-3 ps (Figure 4h), and a kinetic fit with a sigmoid function provides a time-constant of 2.3 ± 0.6 ps for the final $v = 1 \rightarrow v = 0$ cooling step in 9H-Ade. It is notable that these cooling timescales for 9H-Ade are both ~300-400 fs slower than those observed for Ade[-H]$^-$ (see Table 1), indicative of the stronger solvation environment experienced by aqueous anions, relative to neutrals. In stark contrast, the combined 7H-Ade ν_{rs} and ν_{scis} bleach depths plotted in Figure 4h (red) simply display an exponential recovery with a time-constant of 5.5 ± 2.0 ps. This value mirrors the decay of 7H-Ade's excited state,

in-line with the fact that vibrational cooling in D_2O will be faster than IC back to S_0 (~2 ps *vs* ~5-10 ps).

Closer inspection of the bleach recovery traces in Figure 4h shows ~5% of this signal does not fully recover, verified by the TVA spectra at t = 30 ps in Figure 4f (light grey). This observation accords with the formation of photoproducts. In Section 3C, we identified a clear IR signature for Ade[-H] radicals, and calculated IR spectra for both Ade^+ cation species suggest that they should carry IR signatures that are distinct from the radical (some of which may overlap with Ade bleaches), as shown in Figure 5b. However, within the signal-to-noise of our measurements, no obvious product features are found in our TVA spectra, which reflects the small photoproduct quantum yield (≤5%) at 266 nm. The small quantum yield also suggests that the photoproduct(s) must carry a sufficiently strong electronic absorption cross-section around ~350 nm to enable detection with TEAS. At this stage we are still unable to distinguish between Ade^+ and Ade[-H] photoproducts born through ionization and/or N-H bond cleavage mechanisms, respectively.

F. Transient Absorption of Adenine at 220 nm

The results of TEAS and TVAS studies on Ade in D_2O at 220 nm are collated in Figure 6. The chirp-corrected TEA spectra, after subtraction of a D_2O solvent response, are presented in Figure 6a and are similar to those observed for aqueous Ade at 266 nm. The observed ESA signal decays away completely, within the first 20 ps, to leave the same persistent signatures of a photoproduct and e^-_{aq} seen at 266 nm (Figure 4b). Even at this much shorter excitation wavelength, the ESA signal is still found to decay bi-exponentially with time-constants of 230 ± 50 fs and 5.1 ± 2.8 ps, associated with 9H-Ade and 7H-Ade, respectively. Temps and co-workers previously observed this bi-exponential decay to persist down to 245 nm (the shortest wavelength studied by these authors).[49] However, theory suggests that the barrier to

relaxation (located at a $^1\pi\pi^*/^1n\pi^*$ conical intersection) along the required $^1\pi\pi^* \rightarrow {}^1n\pi^* \rightarrow S_0$ pathway in gas phase 7H-Ade should be surmountable at >4.97 eV (<249 nm),[16] and it is surprising that even by 220 nm the 7H tautomer still exhibits a picosecond lifetime. We envisage that a reduction in 7H-Ade's lifetime is still not observed by 220 nm may occur for a number of reasons. (i) After excitation, flux is not initially localized in the correct co-ordinate to transition over this barrier towards the eventual $^1n\pi^*/S_0$ conical intersection. Instead, intramolecular vibrational energy redistribution must first occur (on the order of picoseconds) before this pathway can be accessed. If this scenario were true, it would further highlight that, unless the available relaxation pathway is truly barrierless (*viz*. 9H-Ade), excited state flux must first be channeled into the correct degree of freedom to pass through the necessary transition state(s) en-route to the conical intersection. (ii) Alternatively, the predicted pathway for excited state relaxation of 7H-Ade in the gas phase may be significantly modified in aqueous solution, and any barriers along the necessary coordinates may be increased.

Figure 6c shows TVA spectra obtained from excitation of Ade at 220 nm. The TVA spectra contain the same features observed previously at 266 nm and are analyzed using the same methods detailed in Section 3E. Table 1 shows that time-constants extracted for the evolution of these features are identical (within standard error) to those at 266 nm for 9H-Ade and 7H-Ade (see Figure S4 for extracted kinetic traces). At this shorter wavelength, the extracted bleach recovery traces return a larger photoproduct quantum yield of ~10%, similar to Ade[-H]$^-$. Most importantly though, a single new positive signal is observed in the TVA spectra, centered at ~1530 cm^{-1}, on the blue edge of the 7H-Ade ν_{rs} bleach at t > 5 ps. Comparison with our measurements on Ade[-H]$^-$ reveal that this band cannot be assigned to the Ade[-H] radical, which absorbs at ~1550 cm^{-1} and ~1587 cm^{-1}. No positive features are observed at these locations, strongly indicating that N(9/7)–H bond fission is not active after

excitation of aqueous Ade, even by 220 nm. Instead, we assign this new feature at ~1530 cm^{-1}, and the photoproduct signal at ~350 nm in TEAS at 220 and 266 nm, to formation of the Ade^+ cation. Based on the excess of 9H tautomer in D_2O and small photoproduct yield of ~10%, this will most likely be the 9H-Ade^+ cation. Reference to the calculated spectra in Figure 5b further support this assignment, which predicts a ν_{rs} mode of gas phase 9H-Ade^+ at 1531 cm^{-1}. However, no clear signature for the stronger 9H-Ade^+ ν_{scis} vibration is seen here, which is predicted at ~1621 cm^{-1} and will be directly overlapped with the ν_{scis} bleach of 9H- and 7H-Ade at 1622 cm^{-1}. The positive 9H-Ade^+ ν_{rs} feature only appears after t = 5 ps, although this feature is expected to be present within the first ~100 fs because two-photon ionization should only occur within the duration of the pump pulse. This apparently 'slow' appearance of 9H-Ade^+ is attributed to overlap of the 1530 cm^{-1} band with the adjacent ν_{rs} bleach of 7H-Ade, which hinders its observation until after the bleach has recovered (~8 ps, see Table 1).

4. Discussion

The above analysis of our TEAS and TVAS measurements, leads us to conclude that N–H bond fission in aqueous Ade is not active (with any significant quantum yield) following excitation at either 266 or 220 nm (*via* either homolytic or EDHE driven pathways). We now consider this conclusion within the context of previous experimental and theoretical investigations of Ade in both the gas phase and aqueous solution. H(Rydberg) atom photofragment translational spectroscopy measurements by Nix *et al*. identified the onset for $^1\pi\sigma^*$ mediated N9–H bond fission in isolated 9H-Ade as ≤233 nm (≥5.3 eV),[43] in agreement with findings from the most recent time-resolved studies in the gas phase.[39, 44] In aqueous solution, fluorescence up-conversion experiments by Temps and co-workers hinted that this dissociation channel may become active at much longer wavelengths of ≤266 nm, albeit a

rather tentative deduction.[49] Our observations from TEAS and TVAS, instead imply that no such bond fission channel participates in either aqueous 7H- or 9H-Ade down to 220 nm, as inferred by an absence of any spectral signature for Ade[-H] radical photoproducts.

In principle, the absence of any Ade[-H] radicals in our TVAS and TEAS on aqueous Ade may have a number of origins, which we discuss and consider in-turn. First, unlike the gas phase, the presence of the D_2O solvent can give rise to strong caging effects in the initial wake of any N–H bond fission, leading to rapid geminate recombination of the Ade parent molecule and/or the formation of adducts (*cf.* Refs 87 and 88). In the extreme case where all (or a large fraction of) Ade[-H] + H photoproducts undergo geminate recombination, it would mean that no Ade[-H] species persist within the temporal window of our measurements and any fleeting spectral signature for these photoproducts within the first ~500 fs would be obscured by those of the Ade parent in both TEAS and TVAS. However, comparison with gas phase measurements indicate that at the threshold for this dissociation channel, the H-atoms that partner Ade[-H] are ballistically ejected with high kinetic energies of ~8300 cm^{-1}.[43] Given this observation and the mobile nature of these H-atoms, conventional wisdom would suggest that a significant fraction will escape the solvent cage (as observed in similar systems[89, 90]), leaving behind a sufficient number of Ade[-H] radicals for detection in TEAS and TVAS. Alternatively, the absence of any photoproducts from N-H bond fission down to 220 nm may be due to another solvent induced effect: ultrafast VET from electronically excited Ade to the D_2O solvent bath. Ultrafast quenching of excess vibrational energy (on the order of 100s fs) within electronically excited states to a level below the $^1\pi\pi^*/^1\pi\sigma^*$ conical intersection may prevent any population coupling onto the $^1\pi\sigma^*$ surface. In the absence of any tunneling below the $^1\pi\pi^*/^1\pi\sigma^*$ conical intersection, this process would terminate N–H bond fission, analogous to findings in *p*-methylthioanisole.[91] Once again though, comparison with gas phase measurements allows us to rule out this possibility with some confidence,

which suggests that N–H bond fission should occur within ~100 fs[44] and be kinetically competitive with any ultrafast VET quenching process. Finally, we return to our original conclusion; the absence of Ade[-H] radical photoproducts in our TEAS and TVAS implies that no such N–H bond cleavage channel participates in either 7H- or 9H-Ade down to 220 nm, and that if an onset for this channel exists in aqueous Ade, it must be significantly blue-shifted relative to the gas phase threshold of 233 nm.[43] This general conclusion is also supported by theoretical work on aqueous Ade. Although prior computational studies of aqueous Ade dynamics largely focused on ultrafast relaxation *via* ring-puckering $^1\pi\pi^*/S_0$ conical intersections,[24, 25, 27, 30] Yamazaki and Kato considered the effects of aqueous solvation on 9H-Ade's $^1\pi\sigma^*$ state.[18] This work concluded that the $^1\pi\sigma^*$ state and associated $^1\pi\pi^*/^1\pi\sigma^*$ conical intersection, are destabilized relative to the gas phase by up to ~0.2 eV.[18] Very recent time-dependent density functional theory calculations of aqueous 9H-Ade implied that this state may be even further blue-shifted in water, lying at >6 eV.[31] Based on our current experimental observations and these theoretical calculations, it may be interesting in future experiments to see whether $^1\pi\sigma^*$ driven N-H bond fission in aqueous Ade becomes active at the much shorter wavelength of 200 nm (6.2 eV) – work towards testing this suggestion is currently underway in our laboratory.

As with many other heteroaromatic molecules,[33, 34] the $^1\pi\sigma^*$ state of 9H-Ade will predominantly exhibit 3s Rydberg character (associated with the N9 atom) in the vertical Franck-Condon region, which evolves into repulsive valence character upon extension of the N9–H bond. This strong Rydberg character means that the $^1\pi\sigma^*$ state is both highly diffuse and polarizable, which will play a central role in its solvation. To close, we more broadly consider two of the major effects of solvation which will influence the relative energy of Ade's $^1\pi\sigma^*$ state in D_2O, given its known Rydberg character. First, calculations on related species suggest that electrostatic effects from the solvent could play an important role in

determining the relative energy of the $^1\pi\sigma^*$ states (*cf.* work on phenol and thiophenols[89, 90]), and this aspect of solvation should generally lower the energy of the $^1\pi\sigma^*$ state.[92] Second, the diffuse Rydberg nature of the $^1\pi\sigma^*$ state will render it highly susceptible to Pauli repulsion,[90, 92] through interactions with solvent electron density in the dense and strongly hydrogen-bonded D_2O solvent network that surrounds Ade. This effect will destabilize the $^1\pi\sigma^*$ state. Based on our above experimental findings, we suggest that Pauli repulsion from the solvent is likely to be the dominant effect felt by Ade's $^1\pi\sigma^*$ state upon solvation in D_2O (particularly in the vertical Franck-Condon region), which appears to be strongly blue-shifted relative to the gas phase. Although we acknowledge that there are likely to be additional nuances to this simplistic picture of solvation, this trend might map through for aqueous solvation of $^1\pi\sigma^*$ states in many other heteroaromatic species (*e.g.* phenols, pyrroles and indoles).

5. Conclusions

Using a combination of ultrafast transient electronic and vibrational absorption spectroscopy, we have investigated the possibility of $^1\pi\sigma^*$ driven N-H bond fission from Ade in D_2O following photoexcitation at 266 and 220 nm, which would lead to the formation of Ade[-H] radicals. Photodetachment of an electron from the aqueous deprotonated Ade[-H]$^-$ anion, formed under basic conditions (pD = 12.5), was first used to provide clear UV/visible and IR spectral signatures for the Ade[-H] radical photoproduct. From these measurements, Ade[-H] was found to absorb at ~350 nm in the UV and possess IR signatures at 1550 and 1587 cm^{-1}. At excitation wavelengths of both 266 and 220 nm, the Ade[-H]$^-$ anion was also found to possess an ultrashort excited state lifetime of ~450 fs and undergo rapid vibrational cooling in its hot S_0 state within ~4-5 ps, after internal conversion from its excited $^1\pi\pi^*$ state(s).

In line with previous studies on aqueous Ade,[45, 48] we have also identified two excited state lifetimes of ~200 fs and ~5-10 ps using TEAS at both 266 and 220 nm excitation

wavelengths, which are assigned to the 9H and 7H tautomers, respectively. Further support for this assignment is found through TVAS, which reveals that bleach recoveries for 9H-Ade are defined by vibrational cooling (~4 ps) and exhibit distinctive sigmoid-like kinetic profiles, whereas 7H-Ade bleaches recover with simple exponential kinetics that mirror its longer excited state lifetime (~5 ps). In addition to these findings, a photoproduct signal is observed in TEAS between 340 and 360 nm together with e^-_{aq}, the latter forming through two-photon ionization of Ade. Complementary theoretical calculations reveal that electronic absorption spectroscopy alone cannot provide a definitive assignment of the photoproduct signal at 340 – 360 nm, as both Ade[-H] radicals and Ade^+ cations absorb here. TVAS however, shows no signature for the Ade[-H] radical at 1550 and 1587 cm^{-1}. Instead, a single product feature at 1530 cm^{-1} is assigned to 9H-Ade^+ cations. Based on these observations, we conclude that $^1\pi\sigma^*$ mediated N-H bond fission is not an active process in aqueous Ade after excitation at ≥220 nm. Furthermore, if an onset for this channel does exist in aqueous solution, it must be significantly blue-shifted relative to the measured threshold for N9–H bond fission *via* isolated 9H-Ade's $^1\pi\sigma^*$ state in the gas phase (233 nm),[43] in broad agreement with previous theoretical findings.[18, 31]

Acknowledgements

GMR thanks the Ramsay Memorial Trust for the award of a Ramsay Memorial Fellowship, Prof. Martin Paterson (Heriot-Watt) for use of his computational facilities and Dr Vas Stavros (Warwick) for helpful discussions. HM thanks the EPSRC for award of a Doctoral Training Grant studentship. MPG is supported by a Marie-Curie International Incoming Fellowship (PIIF-GA-2012-326988). This work was supported by the European Research Council

through the ERC Advanced Grant 290966 CAPRI and EPSRC *via* Programme Grant EP/G00224X.

References

(1) Sagan, C. Ultraviolet Selection Pressure on Earliest Organisms. *J. Theor. Biol.* **1973,** *39*, 195-200.

(2) Mulkidjanian, A. Y.; Cherepanov, D. A.; Galperin, M. Y. Survival of the Fittest before the Beginning of Life: Selection of the First Oligonucleotide-Like Polymers by Uv Light. *BMC Evol. Biol.* **2003,** *3*, 12.

(3) Balucani, N. Elementary Reactions and Their Role in Gas-Phase Prebiotic Chemistry. *Int. J. Mol. Sci.* **2009,** *10*, 2304-2335.

(4) Crespo-Hernandez, C. E.; Cohen, B.; Hare, P. M.; Kohler, B. Ultrafast Excited-State Dynamics in Nucleic Acids. *Chem. Rev.* **2004,** *104*, 1977-2019.

(5) Middleton, C. T.; de La Harpe, K.; Su, C.; Law, Y. K.; Crespo-Hernandez, C. E.; Kohler, B. DNA Excited-State Dynamics: From Single Bases to the Double Helix. *Annu. Rev. Phys. Chem.* **2009,** *60*, 217-239.

(6) Kleinermanns, K.; Nachtigallova, D.; de Vries, M. S. Excited State Dynamics of DNA Bases. *Int. Rev. Phys. Chem.* **2013,** *32*, 308-342.

(7) Schreier, W. J.; Schrader, T. E.; Koller, F. O.; Gilch, P.; Crespo-Hernandez, C. E.; Swaminathan, V. N.; Carell, T.; Zinth, W.; Kohler, B. Thymine Dimerization in DNA Is an Ultrafast Photoreaction. *Science* **2007,** *315*, 625-629.

(8) Kohler, B. Nonradiative Decay Mechanisms in DNA Model Systems. *J. Phys. Chem. Lett.* **2010,** *1*, 2047-2053.

(9) Barbatti, M.; Aquino, A. J. A.; Szymczak, J. J.; Nachtigallova, D.; Hobza, P.; Lischka, H. Relaxation Mechanisms of Uv-Photoexcited DNA and Rna Nucleobases. *Proc. Natl. Acad. Sci. U.S.A.* **2010,** *107*, 21453-21458.

(10) Yarkony, D. R. Diabolical Conical Intersections. *Rev Mod Phys* **1996,** *68*, 985-1013.

(11) Yarkony, D. R. Conical Intersections: Diabolical and Often Misunderstood. *Acc. Chem. Res.* **1998,** *31*, 511-518.

(12) Marian, C. M. A New Pathway for the Rapid Decay of Electronically Excited Adenine. *J. Chem. Phys.* **2005,** *122*, 104314.

(13) Perun, S.; Sobolewski, A. L.; Domcke, W. Ab Initio Studies on the Radiationless Decay Mechanisms of the Lowest Excited Singlet States of 9h-Adenine. *J. Am. Chem. Soc.* **2005,** *127*, 6257-6265.

(14) Perun, S.; Sobolewski, A. L.; Domcke, W. Photostability of 9h-Adenine: Mechanisms of the Radiationless Deactivation of the Lowest Excited Singlet States. *Chem. Phys.* **2005,** *313*, 107-112.

(15) Blancafort, L. Excited-State Potential Energy Surface for the Photophysics of Adenine. *J. Am. Chem. Soc.* **2006,** *128*, 210-219.

(16) Serrano-Andres, L.; Merchan, M.; Borin, A. C. A Three-State Model for the Photophysics of Adenine. *Chem. Eur. J.* **2006,** *12*, 6559-6571.

(17) Chung, W. C.; Lan, Z. G.; Ohtsuki, Y.; Shimakura, N.; Domcke, W.; Fujimura, Y. Conical Intersections Involving the Dissociative (1)Pi Sigma* State in 9h-Adenine: A Quantum Chemical Ab Initio Study. *Phys Chem Chem Phys* **2007,** *9*, 2075-2084.

(18) Yamazaki, S.; Kato, S. Solvent Effect on Conical Intersections in Excited-State 9h-Adenine: Radiationless Decay Mechanism in Polar Solvent. *J. Am. Chem. Soc.* **2007,** *129*, 2901-2909.

(19) Barbatti, M.; Lischka, H. Nonadiabatic Deactivation of 9h-Adenine: A Comprehensive Picture Based on Mixed Quantum-Classical Dynamics. *J. Am. Chem. Soc.* **2008,** *130*, 6831-6839.

(20) Conti, I.; Di Donato, E.; Negri, F.; Orlandi, G. Revealing Excited State Interactions by Quantum-Chemical Modeling of Vibronic Activities: The R2pi Spectrum of Adenine. *J. Phys. Chem. A* **2009,** *113*, 15265-15275.

(21) Conti, I.; Garavelli, M.; Orlandi, G. Deciphering Low Energy Deactivation Channels in Adenine. *J. Am. Chem. Soc.* **2009,** *131*, 16108-16118.

(22) Serrano-Andres, L.; Merchan, M. Are the Five Natural DNA/Rna Base Monomers a Good Choice from Natural Selection? A Photochemical Perspective. *J. Photochem. Photobiol. C* **2009,** *10*, 21-32.

(23) Hassan, W. M. I.; Chung, W. C.; Shimakura, N.; Koseki, S.; Kono, H.; Fujimura, Y. Ultrafast Radiationless Transition Pathways through Conical Intersections in Photo-Excited 9h-Adenine. *Phys Chem Chem Phys* **2010,** *12*, 5317-5328.

(24) Ludwig, V.; da Costa, Z. M.; do Amaral, M. S.; Borin, A. C.; Canuto, S.; Serrano-Andres, L. Photophysics and Photostability of Adenine in Aqueous Solution: A Theoretical Study. *Chem. Phys. Lett.* **2010,** *492*, 164-169.

(25) Lan, Z. G.; Lu, Y.; Fabiano, E.; Thiel, W. Qm/Mm Nonadiabatic Decay Dynamics of 9h-Adenine in Aqueous Solution. *ChemPhysChem* **2011,** *12*, 1989-1998.

(26) Barbatti, M.; Lan, Z. G.; Crespo-Otero, R.; Szymczak, J. J.; Lischka, H.; Thiel, W. Critical Appraisal of Excited State Nonadiabatic Dynamics Simulations of 9h-Adenine. *J. Chem. Phys.* **2012,** *137*, 22A503.

(27) Mennucci, B.; Toniolo, A.; Tomasi, J. Theoretical Study of the Photophysics of Adenine in Solution: Tautomerism, Deactivation Mechanisms, and Comparison with the 2-Aminopurine Fluorescent Isomer. *J. Phys. Chem. A* **2001,** *105*, 4749-4757.

(28) Plasser, F.; Crespo-Otero, R.; Pederzoli, M.; Pittner, J.; Lischka, H.; Barbatti, M. Surface Hopping Dynamics with Correlated Single-Reference Methods: 9h-Adenine as a Case Study. *J. Chem. Theory Comput.* **2014,** *10*, 1395-1405.

(29) Picconi, D.; Ferrer, F. J. A.; Improta, R.; Lami, A.; Santoro, F. Quantum-Classical Effective-Modes Dynamics of the Pp* -> Np* Decay in 9h-Adenine. A Quadratic Vibronic Coupling Model. *Faraday Discuss.* **2013,** *163*, 223-242.

(30) Mitric, R.; Werner, U.; Wohlgemuth, M.; Seifert, G.; Bonacic-Koutecky, V. Nonadiabatic Dynamics within Time-Dependent Density Functional Tight Binding Method. *J. Phys. Chem. A* **2009,** *113*, 12700-12705.

(31) Chatterley, A. S.; West, C. W.; Roberts, G. M.; Stavros, V. G.; Verlet, J. R. R. Mapping the Ultrafast Dynamics of Adenine onto Its Nucleotide and Oligonucleotides by Time-Resolved Photoelectron Imaging. *J. Phys. Chem. Lett.* **2014,** *5*, 843-848.

(32) Sobolewski, A. L.; Domcke, W.; Dedonder-Lardeux, C.; Jouvet, C. Excited-State Hydrogen Detachment and Hydrogen Transfer Driven by Repulsive ^{1}ps* States: A New Paradigm for Nonradiative Decay in Aromatic Biomolecules. *Phys Chem Chem Phys* **2002,** *4*, 1093-1100.

(33) Ashfold, M. N. R.; King, G. A.; Murdock, D.; Nix, M. G. D.; Oliver, T. A. A.; Sage, A. G. Ps* Excited States in Molecular Photochemistry. *Phys Chem Chem Phys* **2010,** *12*, 1218-1238.

(34) Roberts, G. M.; Stavros, V. G. The Role of Ps* States in the Photochemistry of Heteroaromatic Biomolecules and Their Subunits: Insights from Gas-Phase Femtosecond Spectroscopy. *Chem. Sci.* **2014,** *5*, 1698-1722.

(35) Bisgaard, C. Z.; Satzger, H.; Ullrich, S.; Stolow, A. Excited-State Dynamics of Isolated DNA Bases: A Case Study of Adenine. *ChemPhysChem* **2009,** *10*, 101-110.

(36) Canuel, C.; Mons, M.; Piuzzi, F.; Tardivel, B.; Dimicoli, I.; Elhanine, M. Excited States Dynamics of DNA and Rna Bases: Characterization of a Stepwise Deactivation Pathway in the Gas Phase. *J. Chem. Phys.* **2005,** *122*, 074316.

(37) Ullrich, S.; Schultz, T.; Zgierski, M. Z.; Stolow, A. Direct Observation of Electronic Relaxation Dynamics in Adenine Via Time-Resolved Photoelectron Spectroscopy. *J. Am. Chem. Soc.* **2004,** *126*, 2262-2263.

(38) Satzger, H.; Townsend, D.; Zgierski, M. Z.; Patchkovskii, S.; Ullrich, S.; Stolow, A. Primary Processes Underlying the Photostability of Isolated DNA Bases: Adenine. *Proc. Natl. Acad. Sci. U.S.A.* **2006,** *103*, 10196-10201.

(39) Evans, N. L.; Ullrich, S. Wavelength Dependence of Electronic Relaxation in Isolated Adenine Using Uv Femtosecond Time-Resolved Photoelectron Spectroscopy. *J. Phys. Chem. A* **2010,** *114*, 11225-11230.

(40) Hunig, I.; Plutzer, C.; Seefeld, K. A.; Lowenich, D.; Nispel, M.; Kleinermanns, K. Photostability of Isolated and Paired Nucleobases: N-H Dissociation of Adenine and Hydrogen Transfer in Its Base Pairs Examined by Laser Spectroscopy. *ChemPhysChem* **2004,** *5*, 1427-1431.

(41) Zierhut, M.; Roth, W.; Fischer, I. Dynamics of H-Atom Loss in Adenine. *Phys Chem Chem Phys* **2004,** *6*, 5178-5183.

(42) Wells, K. L.; Roberts, G. M.; Stavros, V. G. Dynamics of H-Loss in Adenine Via the ^{1}ps* State Using a Combination of Ns and Fs Laser Spectroscopy. *Chem. Phys. Lett.* **2007,** *446*, 20-24.

(43) Nix, M. G. D.; Devine, A. L.; Cronin, B.; Ashfold, M. N. R. Ultraviolet Photolysis of Adenine: Dissociation Via the ^{1}ps* State. *J. Chem. Phys.* **2007,** *126*, 124312.

(44) Wells, K. L.; Hadden, D. J.; Nix, M. G. D.; Stavros, V. G. Competing Ps* States in the Photodissociation of Adenine. *J. Phys. Chem. Lett.* **2010,** *1*, 993-996.

(45) Cohen, B.; Hare, P. M.; Kohler, B. Ultrafast Excited-State Dynamics of Adenine and Monomethylated Adenines in Solution: Implications for the Nonradiative Decay Mechanism. *J. Am. Chem. Soc.* **2003,** *125*, 13594-13601.

(46) Chenon, M. T.; Pugmire, R. J.; Grant, D. M.; Panzica, R. P.; Townsend, L. B. C-13 Magnetic-Resonance .26. Quantitative-Determination of Tautomeric Populations of Certain Purines. *J. Am. Chem. Soc.* **1975,** *97*, 4636-4642.

(47) Gonnella, N. C.; Nakanishi, H.; Holtwick, J. B.; Horowitz, D. S.; Kanamori, K.; Leonard, N. J.; Roberts, J. D. Studies of Tautomers and Protonation of Adenine and Its Derivatives by N-15 Nuclear Magnetic-Resonance Spectroscopy. *J. Am. Chem. Soc.* **1983,** *105*, 2050-2055.

(48) West, B. A.; Womick, J. M.; Moran, A. M. Probing Ultrafast Dynamics in Adenine with Mid-Uv Four-Wave Mixing Spectroscopies. *J. Phys. Chem. A* **2011,** *115*, 8630-8637.

(49) Pancur, T.; Schwalb, N. K.; Renth, F.; Temps, F. Femtosecond Fluorescence up-Conversion Spectroscopy of Adenine and Adenosine: Experimental Evidence for the Ps* State? *Chem. Phys.* **2005,** *313*, 199-212.

(50) Cukier, R. I.; Nocera, D. G. Proton-Coupled Electron Transfer. *Annu. Rev. Phys. Chem.* **1998,** *49*, 337-369.

(51) Pluharova, E.; Jungwirth, P.; Bradforth, S. E.; Slavicek, P. Ionization of Purine Tautomers in Nucleobases, Nucleosides, and Nucleotides: From the Gas Phase to the Aqueous Environment. *J. Phys. Chem. B* **2011,** *115*, 1294-1305.

(52) Pluharova, E.; Schroeder, C.; Seidel, R.; Bradforth, S. E.; Winter, B.; Faubel, M.; Slavicek, P.; Jungwirth, P. Unexpectedly Small Effect of the DNA Environment on Vertical Ionization Energies of Aqueous Nucleobases. *J. Phys. Chem. Lett.* **2013,** *4*, 3766-3769.

(53) Buchner, F.; Ritze, H. H.; Lahl, J.; Lubcke, A. Time-Resolved Photoelectron Spectroscopy of Adenine and Adenosine in Aqueous Solution. *Phys Chem Chem Phys* **2013,** *15*, 11402-11408.

(54) Kuimova, M. K.; Gill, P. M. W.; Lin, C. Y.; Matousek, P.; Towrie, M.; Sun, X. Z.; George, M. W.; Parker, A. W. Picosecond Time-Resolved Infrared Study of 2-Aminopurine Ionisation in Solution. *Photochem. Photobiol. Sci.* **2007,** *6*, 949-955.

(55) Elles, C. G.; Rivera, C. A.; Zhang, Y.; Pieniazek, P. A.; Bradforth, S. E. Electronic Structure of Liquid Water from Polarization-Dependent Two-Photon Absorption Spectroscopy. *J. Chem. Phys.* **2009,** *130*, 084501.

(56) Grubb, M. P.; Orr-Ewing, A. J.; Ashfold, M. N. R. Koala: A Program for the Processing and Decomposition of Transient Spectra. *Rev. Sci. Instrum.* **2014,** *85*, 064104.

(57) Glasoe, P. K.; Long, F. A. Use of Glass Electrodes to Measure Acidities in Deuterium Oxide. *J. Phys. Chem.* **1960,** *64*, 188-190.

(58) Tauber, M. J.; Mathies, R. A.; Chen, X. Y.; Bradforth, S. E. Flowing Liquid Sample Jet for Resonance Raman and Ultrafast Optical Spectroscopy. *Rev. Sci. Instrum.* **2003,** *74*, 4958-4960.

(59) Becke, A. D. Density-Functional Thermochemistry .3. The Role of Exact Exchange. *J. Chem. Phys.* **1993,** *98*, 5648-5652.

(60) Lee, C. T.; Yang, W. T.; Parr, R. G. Development of the Colle-Salvetti Correlation-Energy Formula into a Functional of the Electron-Density. *Phys. Rev. B* **1988,** *37*, 785-789.

(61) Adamo, C.; Barone, V. Toward Reliable Density Functional Methods without Adjustable Parameters: The Pbe0 Model. *J. Chem. Phys.* **1999,** *110*, 6158-6170.

(62) Leang, S. S.; Zahariev, F.; Gordon, M. S. Benchmarking the Performance of Time-Dependent Density Functional Methods. *J. Chem. Phys.* **2012,** *136*, 104101.

(63) Frisch, M. J.; Trucks, G. W.; Schlegel, H. B.; Scuseria, G. E.; Robb, M. A.; Cheeseman, J. R.; Scalmani, G.; Barone, V.; Mennucci, B.; Petersson, G. A.; Nakatsuji, H.; Caricato, M.; Li, X.; Hratchian, H. P.; Izmaylov, A. F.; Bloino, J.; Zheng, G.; Sonnenberg, J. L.; Hada, M.; Ehara, M.; Toyota, K.; Fukuda, R.; Hasegawa, J.; Ishida, M.; Nakajima, T.; Honda, Y.; Kitao, O.; Nakai, H.; Vreven, T.; Montgomery, J. A., Jr.; Peralta, J. E.; Ogliaro, F.; Bearpark, M.; Heyd, J. J.; Brothers, E.; Kudin, K. N.; Staroverov, V. N.; Kobayashi, R.; Normand, J.; Raghavachari, K.; Rendell, A.; Burant,

J. C.; Iyengar, S. S.; Tomasi, J.; Cossi, M.; Rega, N.; Millam, N. J.; Klene, M.; Knox, J. E.; Cross, J. B.; Bakken, V.; Adamo, C.; Jaramillo, J.; Gomperts, R.; Stratmann, R. E.; Yazyev, O.; Austin, A. J.; Cammi, R.; Pomelli, C.; Ochterski, J. W.; Martin, R. L.; Morokuma, K.; Zakrzewski, V. G.; Voth, G. A.; Salvador, P.; Dannenberg, J. J.; Dapprich, S.; Daniels, A. D.; Farkas, Ö.; Foresman, J. B.; Ortiz, J. V.; Cioslowski, J.; Fox, D. J. *Gaussian 09*; Gaussian Inc.: Wallingford, Ct, 2009.

(64) Dawson, R. M. C.; Elliott, D.; Elliott, W. H.; Jones, K. M. *Data for Biochemical Research*. Clarendon Press: Oxford, 1959.

(65) Ganguly, S.; Kundu, K. K. Deprotonation Energetics of Adenine, Adenosine, 5'-Adenosine Monophosphate and Adenosine-Triphosphate in Water from Emf and Spectrophotometric Measurements. *J. Solution Chem.* **1994,** *23*, 1227-1246.

(66) Pecourt, J. M. L.; Peon, J.; Kohler, B. Ultrafast Internal Conversion of Electronically Excited Rna and DNA Nucleosides in Water. *J. Am. Chem. Soc.* **2000,** *122*, 9348-9349.

(67) Pecourt, J. M. L.; Peon, J.; Kohler, B. DNA Excited-State Dynamics: Ultrafast Internal Conversion and Vibrational Cooling in a Series of Nucleosides. *J. Am. Chem. Soc.* **2001,** *123*, 10370-10378.

(68) Jou, F. Y.; Freeman, G. R. Temperature and Isotope Effects on the Shape of the Optical-Absorption Spectrum of Solvated Electrons in Water. *J. Phys. Chem.* **1979,** *83*, 2383-2387.

(69) Stepanian, S. G.; Sheina, G. G.; Radchenko, E. D.; Blagoi, Y. P. Theoretical and Experimental Studies of Adenine, Purine and Pyrimidine Isolated Molecule Structure. *J. Mol. Struct.* **1985,** *131*, 333-346.

(70) van Zundert, G. C. P.; Jaeqx, S.; Berden, G.; Bakker, J. M.; Kleinermanns, K.; Oomens, J.; Rijs, A. M. Ir Spectroscopy of Isolated Neutral and Protonated Adenine and 9-Methyladenine. *ChemPhysChem* **2011,** *12*, 1921-1927.

(71) Banyay, M.; Sarkar, M.; Graslund, A. A Library of Ir Bands of Nucleic Acids in Solution. *Biophys. Chem.* **2003,** *104*, 477-488.

(72) Murdock, D.; Harris, S. J.; Luke, J.; Grubb, M. P.; Orr-Ewing, A. J.; Ashfold, M. N. R. Transient Uv Pump-Ir Probe Investigation of Heterocyclic Ring-Opening Dynamics in the Solution Phase: The

Role Played by Nσ* States in the Photoinduced Reactions of Thiophenone and Furanone. *Chem. Sci.* **2014**, accepted.

(73) Zhang, Y. Y.; Chen, J. Q.; Kohler, B. Hydrogen Bond Donors Accelerate Vibrational Cooling of Hot Purine Derivatives in Heavy Water. *J. Phys. Chem. A* **2013,** *117*, 6771-6780.

(74) Evangelista, F. A.; Paul, A.; Schaefer, H. F. Radicals Derived from Adenine: Prediction of Large Electron Affinities with a Considerable Spread. *J. Phys. Chem. A* **2004,** *108*, 3565-3571.

(75) Lyngdoh, R. H. D.; Schaefer, H. F. Elementary Lesions in DNA Subunits: Electron, Hydrogen Atom, Proton, and Hydride Transfers. *Acc. Chem. Res.* **2009,** *42*, 563-572.

(76) Iizumi, S.; Ninomiya, S.; Sekine, M.; Nakata, M. First Observation of Infrared and Uv-Visible Absorption Spectra of Adenine Radical in Low-Temperature Argon Matrices. *J. Mol. Struct.* **2012,** *1025*, 43-47.

(77) Cheng, Q. Y.; Gu, J. D.; Compaan, K. R.; Schaefer, H. F. Hydroxyl Radical Reactions with Adenine: Reactant Complexes, Transition States, and Product Complexes. *Chem. Eur. J.* **2010,** *16*, 11848-11858.

(78) Elles, C. G.; Jailaubekov, A. E.; Crowell, R. A.; Bradforth, S. E. Excitation-Energy Dependence of the Mechanism for Two-Photon Ionization of Liquid H2o and D2o from 8.3 to 12.4 Ev. *J. Chem. Phys.* **2006,** *125*, 044515.

(79) Chen, X. Y.; Larsen, D. S.; Bradforth, S. E.; van Stokkum, I. H. M. Broadband Spectral Probing Revealing Ultrafast Photochemical Branching after Ultraviolet Excitation of the Aqueous Phenolate Anion. *J. Phys. Chem. A* **2011,** *115*, 3807-3819.

(80) Horng, M. L.; Gardecki, J. A.; Papazyan, A.; Maroncelli, M. Subpicosecond Measurements of Polar Solvation Dynamics - Coumarin-153 Revisited. *J. Phys. Chem.* **1995,** *99*, 17311-17337.

(81) Gardecki, J.; Horng, M. L.; Papazyan, A.; Maroncelli, M. Ultrafast Measurements of the Dynamics of Solvation in Polar and Nondipolar Solvents. *J. Mol. Liq.* **1995,** *65*, 49-57.

(82) Bagchi, B.; Jana, B. Solvation Dynamics in Dipolar Liquids. *Chem. Soc. Rev.* **2010,** *39*, 1936-1954.

(83) Crowell, R. A.; Bartels, D. M. Multiphoton Ionization of Liquid Water with 3.0-5.0 Ev Photons. *J. Phys. Chem.* **1996,** *100*, 17940-17949.

(84) Marian, C. M.; Kleinschmidt, M.; Tatchen, J. The Photophysics of 7h-Adenine: A Quantum Chemical Investigation Including Spin-Orbit Effects. *Chem. Phys.* **2008,** *347*, 346-359.

(85) Lin, J.; Yu, C.; Peng, S.; Akiyama, I.; Li, K.; Lee, L. K.; Lebreton, P. R. Ultraviolet Photoelectron Studies of the Ground-State Electronic-Structure and Gas-Phase Tautomerism of Purine and Adenine. *J. Am. Chem. Soc.* **1980,** *102*, 4627-4631.

(86) Trofimov, A. B.; Schirmer, J.; Kobychev, V. B.; Potts, A. W.; Holland, D. M. P.; Karlsson, L. Photoelectron Spectra of the Nucleobases Cytosine, Thymine and Adenine. *J. Phys. B* **2006,** *39*, 305-329.

(87) Harris, S. J.; Murdock, D.; Zhang, Y. Y.; Oliver, T. A. A.; Grubb, M. P.; Orr-Ewing, A. J.; Greetham, G. M.; Clark, I. P.; Towrie, M.; Bradforth, S. E.; Ashfold, M. N. R. Comparing Molecular Photofragmentation Dynamics in the Gas and Liquid Phases. *Phys Chem Chem Phys* **2013,** *15*, 6567-6582.

(88) Zhang, Y. Y.; Oliver, T. A. A.; Das, S.; Roy, A.; Ashfold, M. N. R.; Bradforth, S. E. Exploring the Energy Disposal Immediately after Bond-Breaking in Solution: The Wavelength-Dependent Excited State Dissociation Pathways of Para-Methylthiophenol. *J. Phys. Chem. A* **2013,** *117*, 12125-12137.

(89) Oliver, T. A. A.; Zhang, Y.; Ashfold, M. N. R.; Bradforth, S. E. Linking Photochemistry in the Gas and Solution Phase: S-H Bond Fission in P-Methylthiophenol Following Uv Photoexcitation. *Faraday Discuss.* **2011,** *150*, 439-458.

(90) Zhang, Y. Y.; Oliver, T. A. A.; Ashfold, M. N. R.; Bradforth, S. E. Contrasting the Excited State Reaction Pathways of Phenol and Para-Methylthiophenol in the Gas and Liquid Phases. *Faraday Discuss.* **2012,** *157*, 141-163.

(91) Murdock, D.; Harris, S. J.; Karsili, T. N. V.; Greetham, G. M.; Clark, I. P.; Towrie, M.; Orr-Ewing, A. J.; Ashfold, M. N. R. Photofragmentation Dynamics in Solution Probed by Transient Ir Absorption Spectroscopy: Ps*-Mediated Bond Cleavage in P-Methylthiophenol and P-Methylthioanisole. *J. Phys. Chem. Lett.* **2012,** *3*, 3715-3720.

(92) Truhlar, D. G.; Bradforth, S. E. General Discussion. *Faraday Discuss.* **2012,** *157*, 243-284.

Scheme, Figure and Table Captions

Scheme 1. Molecular structures of the 9H (blue) and 7H (red) tautomers of adenine which can be deprotonated to formed the adenine anion, Ade[-H]$^-$ (green).

Figure 1. Schematic potential energy cuts for the electronic $^1\pi\pi^*$ (^1L_a, ^1L_b and ^1B_b), lowest energy $^1n\pi^*$, $^1\pi\sigma^*$ and S_0 states of isolated (gas-phase) 9H-Ade with respect to elongation of the N9–H bond (see Scheme 1 and inset structure). Potentials are based on those presented in Refs 14 and 43. Inset: Normalized static UV absorption spectra for Ade (blue line) and the Ade[-H]$^-$ anion (green line) in D_2O, recorded under neutral (pD = 7.4) and basic (pD = 12.5) conditions, respectively.

Figure 2. Results of TEAS (a-c) and TVAS (d-e) experiments on Ade[-H]$^-$ in D_2O (6 mM) under basic conditions (pD = 12.5), following excitation at 266 nm ($F \approx 0.3$ mJ cm^{-2}) and a 100 μm sample path length. (a) Two-dimensional false-color intensity plot of chirped corrected TEA spectra between t = –200 fs and 2.5 ps, over a probe wavelength range of 340 – 620 nm. (b) Normalized integrated ESA signal decay trace and associated fit at λ_{probe} = 400 nm. (c) Select long-time TEA spectra between t = 950 fs and 100 ps, together with a representative D_2O solvent only spectrum at t = 500 ps. (d) Two-dimensional false-color intensity plot of TVA spectra between t = 0 and 20 ps, for an IR probe window of 1490 – 1680 cm^{-1}. Given above are the peak assignments in the TVA spectra (see main text), for the observed positive and negative transient absorption features. (e) Peak center shifts of the

ν^*_{scis} and ν^*_{rs} vibrational hot bands and associated kinetic fits. (f) Normalized integrated bleach recovery traces and kinetic fits for the ν_{scis} and ν_{rs} modes.

Figure 3. Results of TEAS (a-c) and TVAS (d-e) experiments on Ade[-H]$^-$ in D_2O (6 mM) under basic conditions (pD = 12.5), following excitation at 220 nm ($F \approx 0.3$ mJ cm^{-2}) and a 100 μm sample path length. (a) Two-dimensional false-color intensity plot of chirped corrected TEA spectra, after subtraction of a D_2O only solvent response, between t = –200 fs and 2.5 ps, over a probe wavelength range of 340 – 620 nm. (b) Select long-time TEA spectra between t = 900 fs and 100 ps, together with a representative D_2O/NaOD solvent only spectrum at t = 200 ps. (c) Calculated (vertical) electronic transition wavelengths and associated transition strengths for aqueous Ade[-H] radicals, at the TD-PBE0/aug-cc-pVTZ level of theory (with a water PCM), together with a representative TEA spectrum at t = 10 ps. (d) Two-dimensional false-color intensity plot of TVA spectra between t = 0 and 20 ps, for an IR probe window of 1490 – 1680 cm^{-1}. Given above are the peak assignments in the TVA spectra (see main text), for the observed positive and negative transient absorption features. (e) Select long-time TVA spectra between t = 17 ps and 100 ps. (f) Calculated IR spectrum for the isolated (gas-phase) Ade[-H] radical, at the B3LYP/6-311+G(d,p) level of theory, between 1490 and 1680 cm^{-1}. (g-i) Calculated ν_{scis} and ν_{rs} vibrational modes and wavenumbers, associated with the calculated spectrum in (f).

Figure 4. Results of TEAS (a-d) and TVAS (e-f) experiments on Ade in D_2O (6 mM) under neutral conditions (pD = 7.4), following excitation at 266 nm ($F \approx 0.3$ mJ cm^{-2}) and a 100 μm sample path length. (a) Two-dimensional false-color intensity plot of chirped corrected TEA spectra between t = –200 fs and 100 ps, over a probe wavelength range of 340 – 620 nm, with

a log scale time axis after 1 ps. (b,c) Normalized integrated ESA signal decay traces and associated fits at (b) λ_{probe} = 580 nm and (c) λ_{probe} = 400 nm, with a log scale time axis after 1.5 ps. (d) Select long-time TEA spectra between *t* = 3.5 ps and 300 ps, together with a representative D_2O solvent only spectrum at *t* = 500 ps. (e) Two-dimensional false-color intensity plot of TVA spectra between *t* = 0 and 20 ps, for an IR probe window of 1490 – 1680 cm^{-1}. Given above are the peak assignments in the TVA spectra (see main text), for the observed positive and negative transient absorption features. (f) Representative fit of a TVA spectrum at *t* = 1 ps, displaying Gaussian basis functions used to model components of the spectrum associated with 7H-Ade and 9H-Ade, as well as vibrationally excited ground state 9H-Ade* (see main text for details). An example TVA spectrum at *t* = 30 ps also highlights the incomplete bleach recoveries. (g) Peak center shift of the 9H-Ade ν^*_{scis} vibrational hot band and associated kinetic fit. (h) Normalized integrated bleach recovery traces and kinetic fits for the 9H-Ade ν_{scis} and 7H-Ade $\nu_{scis} + \nu_{rs}$ modes.

Figure 5. (a) Calculated (vertical) electronic transition wavelengths and associated transition strengths for aqueous 9H-Ade^+ and 7H-Ade^+ cations, at the TD-PBE0/aug-cc-pVTZ level of theory (with a water PCM), together with a representative TEA spectrum of neutral Ade at *t* = 100 ps (266 nm excitation). Also shown for comparison are the calculated Ade[-H] radical transitions (Figure 3c) at the same level of theory. (b) Calculated IR spectra for isolated (gas-phase) 9H-Ade, 7H-Ade, 9H-Ade^+ and 7H-Ade^+, at the B3LYP/6-311+G(d,p) level of theory, between 1490 and 1680 cm^{-1}. (c-e) Calculated ν_{scis} and ν_{rs} vibrational modes and wavenumbers associated with the calculated spectra for 9H- and 7H-Ade shown in (b).

Figure 6. Results of TEAS (a,b) and TVAS (c,d) experiments on Ade in D_2O (6 mM) under neutral conditions (pD = 7.4), following excitation at 220 nm ($F \approx 0.3$ mJ cm^{-2}) and a 100 μm sample path length. (a) Two-dimensional false-color intensity plot of chirped corrected TEA spectra, after subtraction of a D_2O only solvent response, between t = –200 fs and 100 ps, over a probe wavelength range of 340 – 620 nm, with a logarithmic time axis after 1 ps. (b) Select long-time TEA spectra between t = 3 ps and 250 ps, together with a representative D_2O solvent only spectrum at t = 500 ps. (c) Two-dimensional false-color intensity plot of TVA spectra between t = 0 and 20 ps, for an IR probe window of 1490 – 1680 cm^{-1}. Given above are the peak assignments in the TVA spectra (see main text), for the observed positive and negative transient absorption features. (d) Select long-time TVA spectra between t = 17 ps and 100 ps.

Table 1. Time-constants extracted from kinetic analysis of TEAS and TVAS measurements on Ade (pD = 7.4) and Ade[-H]$^-$ (pD = 12.5) in D_2O, following excitation at 266 and 220 nm. Errors correspond to two standard deviations (2σ).

Scheme 1

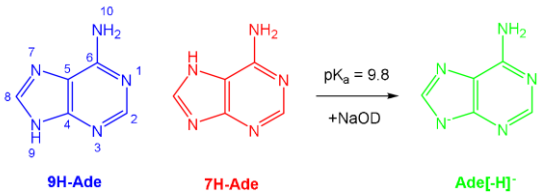

Figure 1

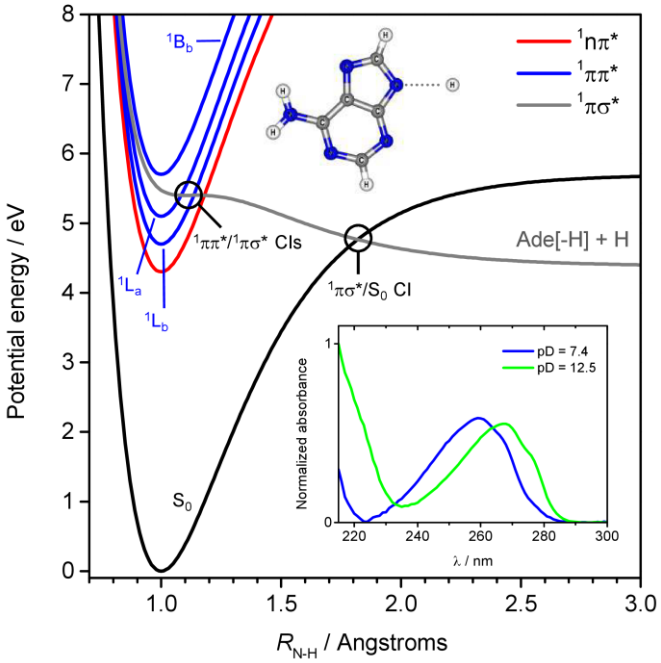
Potential energy / eV
R_{N-H} / Angstroms
^1B_b
^1L_a
^1L_b
$^1\pi\pi^*/^1\pi\sigma^*$ CIs
$^1\pi\sigma^*/S_0$ CI
S_0
Ade[-H] + H
$^1n\pi^*$
$^1\pi\pi^*$
$^1\pi\sigma^*$
Normalized absorbance
pD = 7.4
pD = 12.5
λ / nm

Figure 2

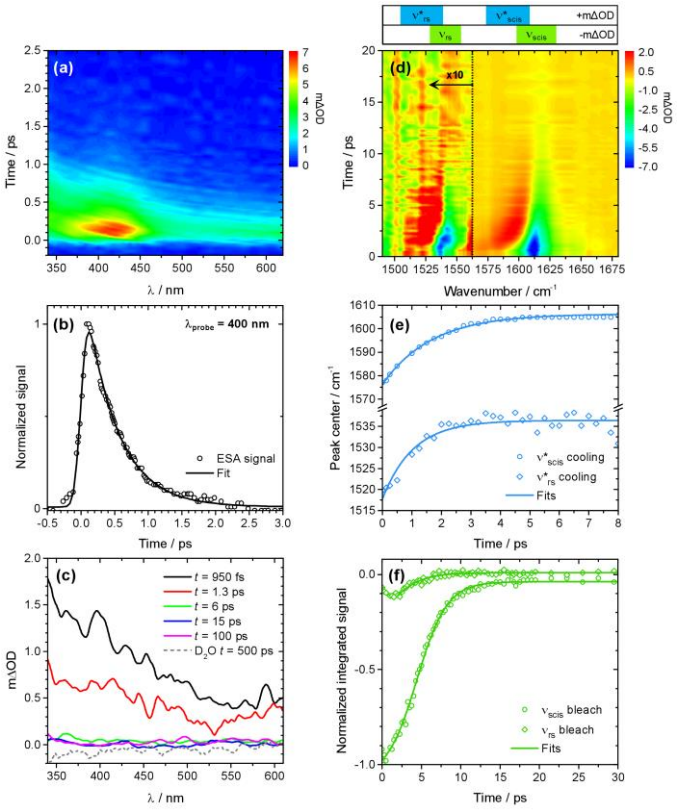
(a)
Time / ps
λ / nm
mΔOD
(b)
λprobe = 400 nm
Normalized signal
ESA signal
Fit
Time / ps
(c)
t = 950 fs
t = 1.3 ps
t = 6 ps
t = 15 ps
t = 100 ps
D2O t = 500 ps
mΔOD
λ / nm
(d)
x10
+mΔOD
-mΔOD
Time / ps
Wavenumber / cm-1
(e)
Peak center / cm-1
ν*scis cooling
ν*rs cooling
Fits
Time / ps
(f)
Normalized integrated signal
νscis bleach
νrs bleach
Fits
Time / ps

Figure 3

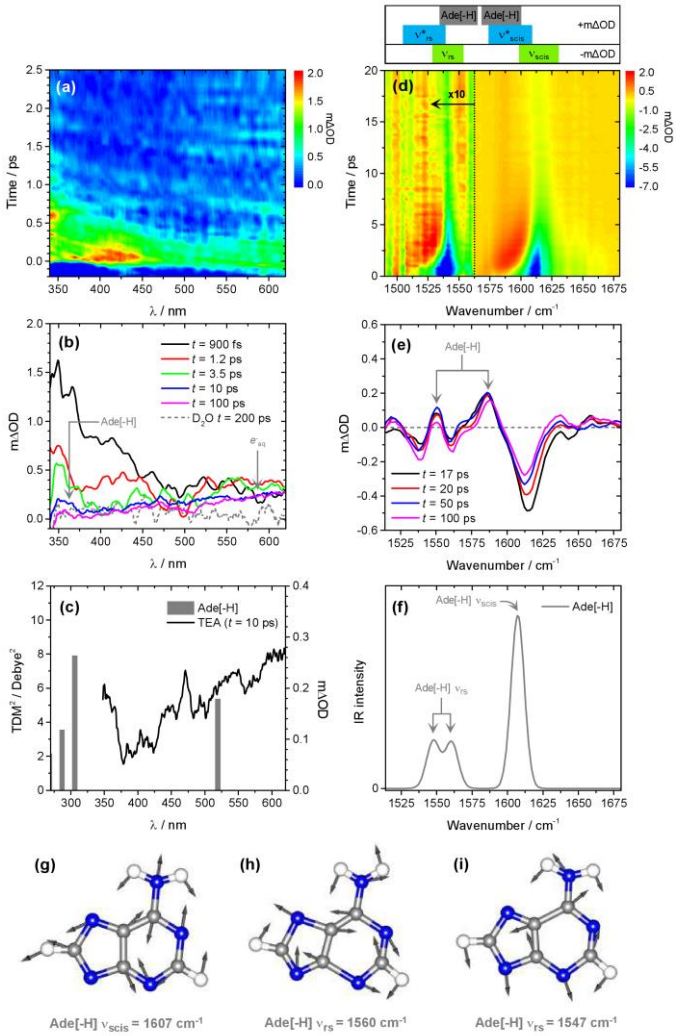
(a)
Time / ps
λ / nm
mΔOD
(b)
t = 900 fs
t = 1.2 ps
t = 3.5 ps
t = 10 ps
t = 100 ps
D2O t = 200 ps
Ade[-H]
mΔOD
λ / nm
(c)
Ade[-H]
TEA (t = 10 ps)
TDM² / Debye²
mΔOD
λ / nm
(d)
x10
+mΔOD
-mΔOD
Time / ps
Wavenumber / cm⁻¹
(e)
Ade[-H]
t = 17 ps
t = 20 ps
t = 50 ps
t = 100 ps
mΔOD
Wavenumber / cm⁻¹
(f)
Ade[-H] νscis
Ade[-H]
Ade[-H] νrs
IR intensity
Wavenumber / cm⁻¹
(g)
Ade[-H] νscis = 1607 cm⁻¹
(h)
Ade[-H] νrs = 1560 cm⁻¹
(i)
Ade[-H] νrs = 1547 cm⁻¹

Figure 4

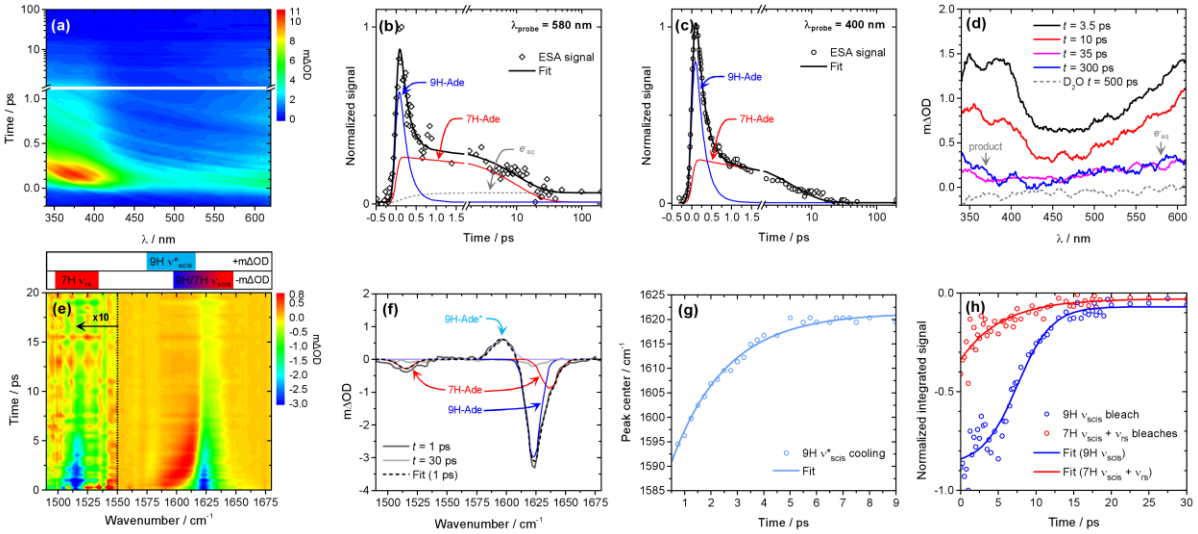
(a)
Time / ps
λ / nm
mΔOD
(b)
λprobe = 580 nm
ESA signal
Fit
9H-Ade
7H-Ade
Normalized signal
Time / ps
(c)
λprobe = 400 nm
ESA signal
Fit
9H-Ade
7H-Ade
Normalized signal
Time / ps
(d)
t = 3.5 ps
t = 10 ps
t = 35 ps
t = 300 ps
D2O t = 500 ps
product
mΔOD
λ / nm
9H ν*scis
+mΔOD
7H νrs
9H/7H νscis
-mΔOD
(e)
x10
Time / ps
Wavenumber / cm-1
mΔOD
(f)
9H-Ade*
7H-Ade
9H-Ade
t = 1 ps
t = 30 ps
Fit (1 ps)
mΔOD
Wavenumber / cm-1
(g)
Peak center / cm-1
9H ν*scis cooling
Fit
Time / ps
(h)
Normalized integrated signal
9H νscis bleach
7H νscis + νrs bleaches
Fit (9H νscis)
Fit (7H νscis + νrs)
Time / ps

Figure 5

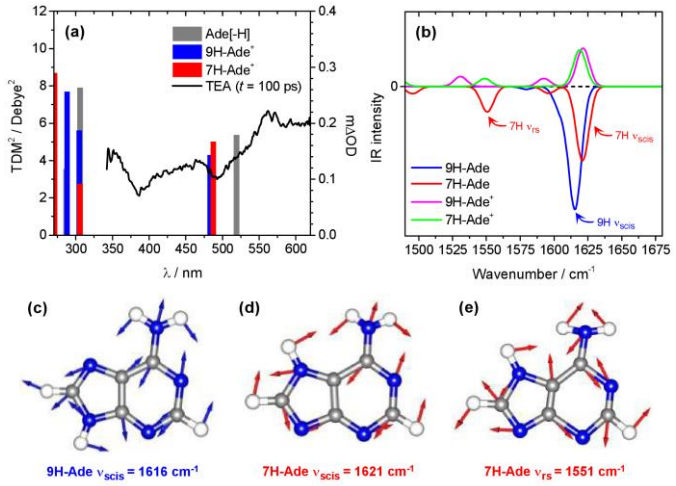
(a)
Ade[-H]
9H-Ade•
7H-Ade•
TEA (t = 100 ps)
TDM² / Debye²
mΔOD
λ / nm
(b)
IR intensity
7H νrs
7H νscis
9H-Ade
7H-Ade
9H-Ade•
7H-Ade•
9H νscis
Wavenumber / cm⁻¹
(c)
9H-Ade νscis = 1616 cm⁻¹
(d)
7H-Ade νscis = 1621 cm⁻¹
(e)
7H-Ade νrs = 1551 cm⁻¹

Figure 6

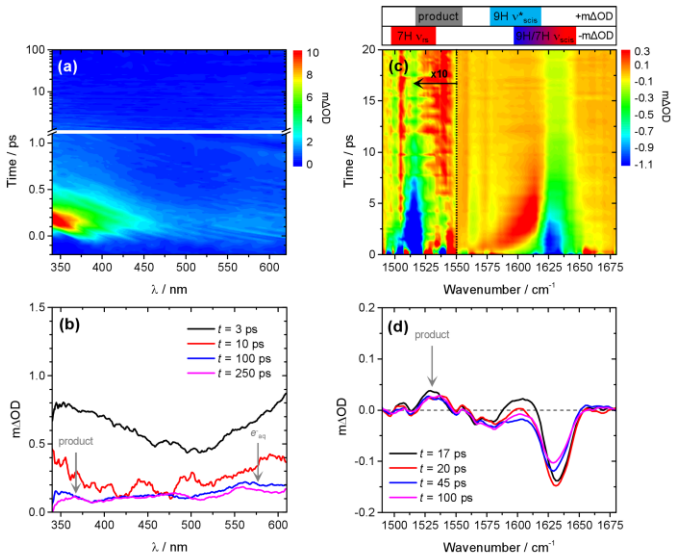
(a)
Time / ps
λ / nm
mΔOD
(c)
x10
product
9H ν*scis
+mΔOD
7H νin
8H/7H νout
-mΔOD
Wavenumber / cm-1
(b)
t = 3 ps
t = 10 ps
t = 100 ps
t = 250 ps
product
mΔOD
(d)
product
t = 17 ps
t = 20 ps
t = 45 ps
t = 100 ps

Table 1

Parameter	266 nm			220 nm		
	Ade[-H]$^-$	9H-Ade	7H-Ade	Ade[-H]$^-$	9H-Ade	7H-Ade
Lifetime (τ_{IC})	470 ± 18 fs	205 ± 14 fs[a]	5.4 ± 0.7 ps[a]	420 ± 22 fs	230 ± 50 fs[a]	5.1 ± 2.8 ps[a]
ν_{rs} recovery	2.2 ± 0.4 ps	-	5.5 ± 2.0 ps[b]	2.0 ± 0.6 ps	-	7.8 ± 2.0 ps[b]
ν^*_{rs} cooling	1.1 ± 0.3 ps	-	-	1.3 ± 0.3 ps	-	-
ν_{scis} recovery	1.9 ± 0.2 ps	2.3 ± 0.6 ps	5.5 ± 2.0 ps[b]	2.0 ± 0.2 ps	2.7 ± 0.4 ps	7.8 ± 2.0 ps[b]
ν^*_{scis} cooling	1.7 ± 0.4 ps	2.1 ± 0.2 ps	-	1.7 ± 0.1 ps	2.1 ± 0.4 ps	-

[a] time-constants extracted from kinetic traces at λ_{probe} = 400 nm. [b] time-constant is extracted from a combined analysis of the 7H-Ade ν_{rs} and ν_{scis} bleaches – see Section 3E.

Cover Art